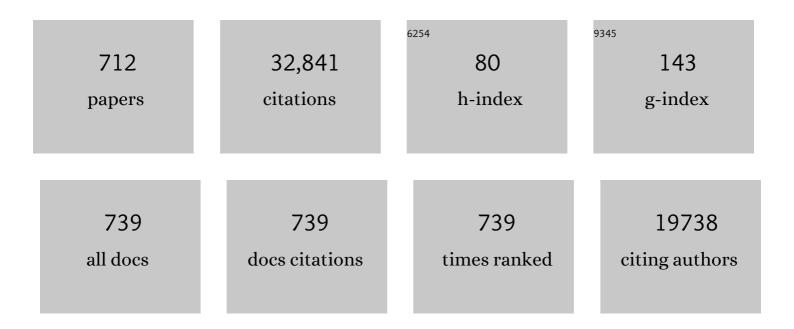
List of Publications by Year in descending order

Source: https://exaly.com/author-pdf/3327625/publications.pdf Version: 2024-02-01



#	Article	IF	CITATIONS
1	Residual stress. Part 1 – Measurement techniques. Materials Science and Technology, 2001, 17, 355-365.	1.6	1,222
2	Friction stir welding of aluminium alloys. International Materials Reviews, 2009, 54, 49-93.	19.3	977
3	Quantitative X-ray tomography. International Materials Reviews, 2014, 59, 1-43.	19.3	975
4	Residual stress. Part 2 – Nature and origins. Materials Science and Technology, 2001, 17, 366-375.	1.6	745
5	Microstructure, mechanical properties and residual stresses as a function of welding speed in aluminium AA5083 friction stir welds. Acta Materialia, 2003, 51, 4791-4801.	7.9	624
6	Residual stress and its role in failure. Reports on Progress in Physics, 2007, 70, 2211-2264.	20.1	571
7	The influence of the laser scan strategy on grain structure and cracking behaviour in SLM powder-bed fabricated nickel superalloy. Journal of Alloys and Compounds, 2014, 615, 338-347.	5.5	539
8	In situ X-ray imaging of defect and molten pool dynamics in laser additive manufacturing. Nature Communications, 2018, 9, 1355.	12.8	495
9	X-ray computed tomography of polymer composites. Composites Science and Technology, 2018, 156, 305-319.	7.8	455
10	Friction stir welding/processing of metals and alloys: A comprehensive review on microstructural evolution. Progress in Materials Science, 2021, 117, 100752.	32.8	436
11	The application of the eshelby method of internal stress determination to short fibre metal matrix composites. Acta Metallurgica, 1989, 37, 3061-3084.	2.1	377
12	X-ray computed tomography. Nature Reviews Methods Primers, 2021, 1, .	21.2	305
13	The Influence of Porosity on Fatigue Crack Initiation in Additively Manufactured Titanium Components. Scientific Reports, 2017, 7, 7308.	3.3	303
14	Influence of processing conditions on strut structure and compressive properties of cellular lattice structures fabricated by selective laser melting. Materials Science & Engineering A: Structural Materials: Properties, Microstructure and Processing, 2015, 628, 188-197.	5.6	289
15	Two-dimensional X-ray CT image based meso-scale fracture modelling of concrete. Engineering Fracture Mechanics, 2015, 133, 24-39.	4.3	289
16	X-ray nanotomography. Materials Today, 2007, 10, 26-34.	14.2	278
17	Large volume serial section tomography by Xe Plasma FIB dual beam microscopy. Ultramicroscopy, 2016, 161, 119-129.	1.9	231
18	Recent advances in residual stress measurement. International Journal of Pressure Vessels and Piping, 2008, 85, 118-127.	2.6	225

#	Article	IF	CITATIONS
19	The effect of powder oxidation on defect formation in laser additive manufacturing. Acta Materialia, 2019, 166, 294-305.	7.9	217
20	The effect of manufacturing defects on the fatigue life of selective laser melted Ti-6Al-4V structures. Materials and Design, 2020, 192, 108708.	7.0	209
21	Porosity regrowth during heat treatment of hot isostatically pressed additively manufactured titanium components. Scripta Materialia, 2016, 122, 72-76.	5.2	207
22	The Effectiveness of Hot Isostatic Pressing for Closing Porosity in Titanium Parts Manufactured by Selective Electron Beam Melting. Metallurgical and Materials Transactions A: Physical Metallurgy and Materials Science, 2016, 47, 1939-1946.	2.2	203
23	Methods for obtaining the strain-free lattice parameter when using diffraction to determine residual stress. Journal of Applied Crystallography, 2007, 40, 891-904.	4.5	194
24	High-temperature strain field measurement using digital image correlation. Journal of Strain Analysis for Engineering Design, 2009, 44, 263-271.	1.8	180
25	Welding residual stresses in ferritic power plant steels. Materials Science and Technology, 2007, 23, 1009-1020.	1.6	176
26	The imaging of failure in structural materials by synchrotron radiation X-ray microtomography. Engineering Fracture Mechanics, 2017, 182, 127-156.	4.3	168
27	Image based modelling of microstructural heterogeneity in LiFePO 4 electrodes for Li-ion batteries. Journal of Power Sources, 2014, 247, 1033-1039.	7.8	162
28	Dissimilar friction stir welds in AA5083–AA6082: The effect of process parameters on residual stress. Materials Science & Engineering A: Structural Materials: Properties, Microstructure and Processing, 2006, 441, 187-196.	5.6	161
29	Residual stress of as-deposited and rolled wire+arc additive manufacturing Ti–6Al–4V components. Materials Science and Technology, 2016, 32, 1439-1448.	1.6	160
30	Ablation-resistant carbide Zr0.8Ti0.2C0.74B0.26 for oxidizing environments up to 3,000 °C. Nature Communications, 2017, 8, 15836.	12.8	154
31	Interphase and intergranular stress generation in carbon steels. Acta Materialia, 2004, 52, 1937-1951.	7.9	149
32	Residual stresses in laser direct metal deposited Waspaloy. Materials Science & Engineering A: Structural Materials: Properties, Microstructure and Processing, 2011, 528, 2288-2298.	5.6	149
33	A machine-learning fatigue life prediction approach of additively manufactured metals. Engineering Fracture Mechanics, 2021, 242, 107508.	4.3	149
34	Time-of-flight neutron transmission diffraction. Journal of Applied Crystallography, 2001, 34, 289-297.	4.5	145
35	The effect of defect population on the anisotropic fatigue resistance of AlSi10Mg alloy fabricated by laser powder bed fusion. International Journal of Fatigue, 2021, 151, 106317.	5.7	144
36	SALSA—A new instrument for strain imaging in engineering materials and components. Materials Science & Engineering A: Structural Materials: Properties, Microstructure and Processing, 2006, 437, 139-144.	5.6	140

#	Article	IF	CITATIONS
37	A high energy synchrotron x-ray study of crystallographic texture and lattice strain in soft lead zirconate titanate ceramics. Journal of Applied Physics, 2004, 96, 4245-4252.	2.5	138
38	Full-field strain mapping by optical correlation of micrographs acquired during deformation. Journal of Microscopy, 2005, 218, 9-21.	1.8	137
39	Dissimilar friction stir welds in AA5083-AA6082. Part I: Process parameter effects on thermal history and weld properties. Metallurgical and Materials Transactions A: Physical Metallurgy and Materials Science, 2006, 37, 2183-2193.	2.2	136
40	Three-dimensional characterization of electrodeposited lithium microstructures using synchrotron X-ray phase contrast imaging. Chemical Communications, 2015, 51, 266-268.	4.1	133
41	A new approach to correlate the defect population with the fatigue life of selective laser melted Ti-6Al-4V alloy. International Journal of Fatigue, 2020, 136, 105584.	5.7	133
42	Fatigue and Damage in Structural Materials Studied by X-Ray Tomography. Annual Review of Materials Research, 2012, 42, 81-103.	9.3	129
43	Correlative Tomography. Scientific Reports, 2014, 4, 4711.	3.3	124
44	Strain imaging by Bragg edge neutron transmission. Nuclear Instruments and Methods in Physics Research, Section A: Accelerators, Spectrometers, Detectors and Associated Equipment, 2002, 481, 765-768.	1.6	119
45	Multi Length Scale Microstructural Investigations of a Commercially Available Li-Ion Battery Electrode. Journal of the Electrochemical Society, 2012, 159, A1023-A1027.	2.9	118
46	Texture development in Ti–6Al–4V linear friction welds. Materials Science & Engineering A: Structural Materials: Properties, Microstructure and Processing, 2007, 459, 182-191.	5.6	117
47	The determination of the elastic field of an ellipsoidal inclusion in a transversely isotropic medium, and its relevance to composite materials. Philosophical Magazine A: Physics of Condensed Matter, Structure, Defects and Mechanical Properties, 1989, 59, 759-781.	0.6	116
48	A combined approach to microstructure mapping of an Al–Li AA2199 friction stir weld. Acta Materialia, 2011, 59, 3002-3011.	7.9	115
49	Non-destructive mapping of grain orientations in 3D by laboratory X-ray microscopy. Scientific Reports, 2015, 5, 14665.	3.3	114
50	Characterizing Phase Transformations and Their Effects on Ferritic Weld Residual Stresses with X-Rays and Neutrons. Metallurgical and Materials Transactions A: Physical Metallurgy and Materials Science, 2008, 39, 3070-3078.	2.2	111
51	The stress intensity of mixed mode cracks determined by digital image correlation. Journal of Strain Analysis for Engineering Design, 2008, 43, 769-780.	1.8	111
52	The analysis of internal strains measured by neutron diffraction in Al/SiC metal matrix composites. Acta Metallurgica Et Materialia, 1992, 40, 2361-2373.	1.8	108
53	Three dimensional observations and modelling of intergranular stress corrosion cracking in austenitic stainless steel. Journal of Nuclear Materials, 2006, 352, 62-74.	2.7	108
54	The effect of defects on the mechanical response of Ti-6Al-4V cubic lattice structures fabricated by electron beam melting. Acta Materialia, 2016, 108, 279-292.	7.9	108

#	Article	IF	CITATIONS
55	Application of Micro-Computed Tomography With Iodine Staining to Cardiac Imaging, Segmentation, and Computational Model Development. IEEE Transactions on Medical Imaging, 2013, 32, 8-17.	8.9	106
56	Microstructure mapping in friction stir welds of 7449 aluminium alloy using SAXS. Acta Materialia, 2006, 54, 4793-4801.	7.9	104
57	Separation of macroscopic, elastic mismatch and thermal expansion misfit stresses in metal matrix composite quenched plates from neutron diffraction measurements. Acta Materialia, 1997, 45, 4867-4876.	7.9	103
58	On the deformation twinning of Mg AZ31B: A three-dimensional synchrotron X-ray diffraction experiment and crystal plasticity finite element model. International Journal of Plasticity, 2015, 70, 77-97.	8.8	103
59	Comparison of tool wear mechanisms and surface integrity for dry and wet micro-drilling of nickel-base superalloys. International Journal of Machine Tools and Manufacture, 2014, 76, 49-60.	13.4	101
60	2D and 3D imaging of fatigue failure mechanisms of 3D woven composites. Composites Part A: Applied Science and Manufacturing, 2015, 77, 37-49.	7.6	100
61	Residual stress driven creep cracking in AISI Type 316 stainless steel. Acta Materialia, 2008, 56, 3598-3612.	7.9	99
62	Deformation twinning in Ti-6Al-4V during low strain rate deformation to moderate strains at room temperature. Materials Science & Engineering A: Structural Materials: Properties, Microstructure and Processing, 2010, 527, 5734-5744.	5.6	95
63	X-ray computed tomography in life sciences. BMC Biology, 2020, 18, 21.	3.8	95
64	Weibull modelling of particle cracking in metal matrix composites. Acta Metallurgica Et Materialia, 1995, 43, 3685-3699.	1.8	94
65	Evolution of a laser shock peened residual stress field locally with foreign object damage and subsequent fatigue crack growth. Acta Materialia, 2015, 83, 216-226.	7.9	94
66	Linking microstructure and processing defects to mechanical properties of selectively laser melted AlSi10Mg alloy. Theoretical and Applied Fracture Mechanics, 2018, 98, 123-133.	4.7	92
67	High resolution X-ray tomography of short fatigue crack nucleation in austempered ductile cast iron. International Journal of Fatigue, 2004, 26, 717-725.	5.7	91
68	X-ray microtomographic observation of intergranular stress corrosion cracking in sensitised austenitic stainless steel. Materials Science and Technology, 2006, 22, 1068-1075.	1.6	91
69	Damage development in open-hole composite specimens in fatigue. Part 1: Experimental investigation. Composite Structures, 2013, 106, 882-889.	5.8	90
70	Lithiationâ€Induced Dilation Mapping in a Lithiumâ€Ion Battery Electrode by 3D Xâ€Ray Microscopy and Digital Volume Correlation. Advanced Energy Materials, 2014, 4, 1300506.	19.5	89
71	Engineering applications of Bragg-edge neutron transmission. Applied Physics A: Materials Science and Processing, 2002, 74, s1433-s1436.	2.3	88
72	Residual stress engineering in friction stir welds by roller tensioning. Science and Technology of Welding and Joining, 2009, 14, 185-192.	3.1	88

#	Article	IF	CITATIONS
73	The effect of particle distribution on damage formation in particulate reinforced metal matrix composites deformed in compression. Materials Science & Engineering A: Structural Materials: Properties, Microstructure and Processing, 1996, 220, 41-56.	5.6	87
74	Importance of crystal orientation in linear friction joining of single crystal to polycrystalline nickel-based superalloys. Materials Science & Engineering A: Structural Materials: Properties, Microstructure and Processing, 2008, 491, 446-453.	5.6	86
75	Synchrotron X-ray studies of austenite and bainitic ferrite. Proceedings of the Royal Society A: Mathematical, Physical and Engineering Sciences, 2008, 464, 1009-1027.	2.1	86
76	Morphological Characterisation of Unstained and Intact Tissue Micro-architecture by X-ray Computed Micro- and Nano-Tomography. Scientific Reports, 2015, 5, 10074.	3.3	86
77	Corrosion fatigue lifetime assessment of high-speed railway axle EA4T steel with artificial scratch. Engineering Fracture Mechanics, 2021, 245, 107588.	4.3	86
78	Global mechanical tensioning for the management of residual stresses in welds. Materials Science & Engineering A: Structural Materials: Properties, Microstructure and Processing, 2008, 489, 351-362.	5.6	85
79	Evolution of damage during the fatigue of 3D woven glass-fibre reinforced composites subjected to tension–tension loading observed by time-lapse X-ray tomography. Composites Part A: Applied Science and Manufacturing, 2016, 82, 279-290.	7.6	85
80	Inertia welding nickel-based superalloy: Part I. Metallurgical characterization. Metallurgical and Materials Transactions A: Physical Metallurgy and Materials Science, 2002, 33, 3215-3225.	2.2	84
81	Neutron and synchrotron measurements of residual strain in TIG welded aluminium alloy 2024. Materials Science & Engineering A: Structural Materials: Properties, Microstructure and Processing, 2003, 346, 159-167.	5.6	84
82	Region-of-interest tomography using filtered backprojection: assessing the practical limits. Journal of Microscopy, 2011, 241, 69-82.	1.8	83
83	Crystallographic effects on the corrosion of twin roll cast AZ31 Mg alloy sheet. Acta Materialia, 2017, 133, 90-99.	7.9	83
84	A comparison of inertia friction welds in three nickel base superalloys. Materials Science & Engineering A: Structural Materials: Properties, Microstructure and Processing, 2006, 437, 38-45.	5.6	82
85	The sensitivity of Ni-based superalloy to hole making operations: Influence of process parameters on subsurface damage and residual stress. Journal of Materials Processing Technology, 2009, 209, 3968-3977.	6.3	82
86	Investigation of strain-rate effect on the compressive behaviour of closed-cell aluminium foam by 3D image-based modelling. Materials and Design, 2016, 89, 215-224.	7.0	82
87	The evolution of crack-tip stresses during a fatigue overload event. Acta Materialia, 2010, 58, 4039-4052.	7.9	81
88	Metamorphosis revealed: time-lapse three-dimensional imaging inside a living chrysalis. Journal of the Royal Society Interface, 2013, 10, 20130304.	3.4	80
89	The effect of density and feature size on mechanical properties of isostructural metallic foams produced by additive manufacturing. Acta Materialia, 2015, 85, 387-395.	7.9	80
90	Repeated crack healing in MAX-phase ceramics revealed by 4D in situ synchrotron X-ray tomographic microscopy. Scientific Reports, 2016, 6, 23040.	3.3	80

#	Article	IF	CITATIONS
91	Relaxation of residual stress in shot peened Udimet 720Li under high temperature isothermal fatigue. International Journal of Fatigue, 2005, 27, 1530-1534.	5.7	78
92	Mapping two-dimensional state of strain using synchroton X-ray diffraction. Scripta Materialia, 1998, 39, 1705-1712.	5.2	77
93	The effect of $\hat{l}^2$ phase on microstructure and texture evolution during thermomechanical processing of $\hat{l}_{\pm}$ + $\hat{l}^2$ Ti alloy. Acta Materialia, 2013, 61, 3200-3213.	7.9	77
94	Comparison of residual stress distributions in conventional and stationary shoulder high-strength aluminum alloy friction stir welds. Journal of Materials Processing Technology, 2017, 242, 92-100.	6.3	77
95	Neutron and Synchrotron Xâ€ <b>r</b> ay Strain Scanning. Strain, 2001, 37, 19-33.	2.4	76
96	Analysis of elastic strain and crystallographic texture in poled rhombohedral PZT ceramics. Acta Materialia, 2006, 54, 3075-3083.	7.9	76
97	Using Synchrotron X-Ray Nano-CT to Characterize SOFC Electrode Microstructures in Three-Dimensions at Operating Temperature. Electrochemical and Solid-State Letters, 2011, 14, B117.	2.2	76
98	The Measurement of Residual Stress in Railway Rails by Diffraction and other Methods *. Journal of Neutron Research, 2003, 11, 187-193.	1.1	75
99	Comparison of residual stresses in Ti–6Al–4V and Ti–6Al–2Sn–4Zr–2Mo linear friction welds. Materials Science and Technology, 2009, 25, 640-650.	1.6	74
100	Generation of micro-scale finite element models from synchrotron X-ray CT images for multidirectional carbon fibre reinforced composites. Composites Part A: Applied Science and Manufacturing, 2016, 91, 85-95.	7.6	74
101	Noncontact Characterization of Carbon-Fiber-Reinforced Plastics Using Multifrequency Eddy Current Sensors. IEEE Transactions on Instrumentation and Measurement, 2009, 58, 738-743.	4.7	73
102	The application of phase contrast X-ray techniques for imaging Li-ion battery electrodes. Nuclear Instruments & Methods in Physics Research B, 2014, 324, 118-123.	1.4	73
103	Completing the picture through correlative characterization. Nature Materials, 2019, 18, 1041-1049.	27.5	73
104	Effects of fatigue and fretting on residual stresses introduced by laser shock peening. Materials Science & Engineering A: Structural Materials: Properties, Microstructure and Processing, 2006, 435-436, 12-18.	5.6	72
105	3D chemical imaging in the laboratory by hyperspectral X-ray computed tomography. Scientific Reports, 2015, 5, 15979.	3.3	72
106	Fracture mechanics by three-dimensional crack-tip synchrotron X-ray microscopy. Philosophical Transactions Series A, Mathematical, Physical, and Engineering Sciences, 2015, 373, 20130157.	3.4	72
107	The potency of defects on fatigue of additively manufactured metals. International Journal of Mechanical Sciences, 2022, 221, 107185.	6.7	72
108	High-resolution strain mapping in bulk samples using full-profile analysis of energy-dispersive synchrotron X-ray diffraction data. Journal of Applied Crystallography, 2004, 37, 883-889.	4.5	71

#	Article	IF	CITATIONS
109	Engineering the residual stress state and microstructure ofÂstainless steel with mechanical surface treatments. Applied Physics A: Materials Science and Processing, 2010, 99, 549-556.	2.3	71
110	The variation in elastic modulus throughout the compression of foam materials. Acta Materialia, 2016, 110, 161-174.	7.9	71
111	Mapping fibre failure in situ in carbon fibre reinforced polymers by fast synchrotron X-ray computed tomography. Composites Science and Technology, 2017, 149, 81-89.	7.8	71
112	Dissimilar friction stir welds in AA5083-AA6082. Part II: Process parameter effects on microstructure. Metallurgical and Materials Transactions A: Physical Metallurgy and Materials Science, 2006, 37, 2195-2206.	2.2	70
113	Mapping residual and internal stress in materials by neutron diffraction. Comptes Rendus Physique, 2007, 8, 806-820.	0.9	70
114	Crystallographic texture and microstructure of pulsed diode laser-deposited Waspaloy. Acta Materialia, 2009, 57, 1220-1229.	7.9	70
115	X-ray computed tomography study of kink bands in unidirectional composites. Composite Structures, 2017, 160, 917-924.	5.8	69
116	Neutron-diffraction study of stress-induced martensitic transformation in TRIP steel. Applied Physics A: Materials Science and Processing, 2002, 74, s1143-s1145.	2.3	68
117	X-ray damage characterisation in self-healing fibre reinforced polymers. Composites Part A: Applied Science and Manufacturing, 2012, 43, 613-620.	7.6	68
118	Exploring microstructural changes associated with oxidation in Ni–YSZ SOFC electrodes using high resolution X-ray computed tomography. Solid State Ionics, 2012, 216, 69-72.	2.7	68
119	The effect of tensioning and sectioning on residual stresses in aluminium AA7749 friction stir welds. Materials Science & Engineering A: Structural Materials: Properties, Microstructure and Processing, 2008, 488, 16-24.	5.6	66
120	A novel architecture for pore network modelling with applications to permeability of porous media. Journal of Hydrology, 2013, 486, 246-258.	5.4	66
121	A neutron diffraction study of load partitioning in continuous Ti/SiC composites. Acta Materialia, 1998, 46, 6585-6598.	7.9	64
122	On the evolution of local material properties and residual stress in a three-pass SA508 steel weld. Acta Materialia, 2012, 60, 3268-3278.	7.9	64
123	Some experimental observations on crack closure and crackâ€ŧip plasticity. Fatigue and Fracture of Engineering Materials and Structures, 2009, 32, 418-429.	3.4	63
124	Evaluation of surface integrity in micro drilling process for nickel-based superalloy. International Journal of Advanced Manufacturing Technology, 2011, 55, 465-476.	3.0	63
125	Determination of the high temperature elastic properties and diffraction elastic constants of Ni-base superalloys. Materials and Design, 2016, 89, 856-863.	7.0	63
126	The deformation of discontinuously reinforced MMCs—I. The initial yielding behaviour. Acta Metallurgica Et Materialia, 1994, 42, 3425-3436.	1.8	62

#	Article	IF	CITATIONS
127	Turning of advanced Ni based alloys obtained via powder metallurgy route. CIRP Annals - Manufacturing Technology, 2006, 55, 117-120.	3.6	62
128	Effect of overload on crack closure in thick and thin specimens via digital image correlation. International Journal of Fatigue, 2013, 56, 17-24.	5.7	62
129	The quantification of impact damage distribution in composite laminates by analysis of X-ray computed tomograms. Composites Science and Technology, 2017, 152, 139-148.	7.8	62
130	Defect evolution during high temperature tension-tension fatigue of SLM AlSi10Mg alloy by synchrotron tomography. Materials Science & Engineering A: Structural Materials: Properties, Microstructure and Processing, 2020, 792, 139809.	5.6	62
131	Quantification of creep cavitation damage around a crack in a stainless steel pressure vessel. Acta Materialia, 2004, 52, 23-34.	7.9	60
132	Using pulsed neutron transmission for crystalline phase imaging and analysis. Journal of Applied Physics, 2005, 97, 074903.	2.5	60
133	Synchrotron X-ray residual strain scanning of a friction stir weld. Journal of Strain Analysis for Engineering Design, 2001, 36, 61-70.	1.8	59
134	Micromechanics of residual stress and texture development due to poling in polycrystalline ferroelectric ceramics. Journal of the Mechanics and Physics of Solids, 2005, 53, 249-260.	4.8	59
135	Surface Decoration for Improving the Accuracy of Displacement Measurements by Digital Image Correlation in SEM. Experimental Mechanics, 2012, 52, 793-804.	2.0	59
136	Fatigue damage assessment of uni-directional non-crimp fabric reinforced polyester composite using X-ray computed tomography. Composites Science and Technology, 2016, 136, 94-103.	7.8	59
137	In situ three-dimensional X-ray microtomography of an auxetic foam under tension. Scripta Materialia, 2009, 60, 232-235.	5.2	58
138	Residual stresses in face finish turning of high strength nickel-based superalloy. Journal of Materials Processing Technology, 2009, 209, 4896-4902.	6.3	58
139	Microstructural evolution during sintering of copper particles studied by laboratory diffraction contrast tomography (LabDCT). Scientific Reports, 2017, 7, 5251.	3.3	58
140	Laser-matter interactions in additive manufacturing of stainless steel SS316L and 13-93 bioactive glass revealed by in situ X-ray imaging. Additive Manufacturing, 2018, 24, 647-657.	3.0	57
141	Effect of preheating on the thermal, microstructural and mechanical properties of selective electron beam melted Ti-6Al-4V components. Materials and Design, 2019, 174, 107792.	7.0	57
142	ENGIN — A new instrument for engineers. Physica B: Condensed Matter, 1997, 234-236, 1141-1143.	2.7	56
143	An anisotropic enhanced thermal conductivity approach for modelling laser melt pools for Ni-base super alloys. Applied Mathematical Modelling, 2013, 37, 1187-1195.	4.2	56
144	Modelling the effect of elastic and plastic anisotropies on stresses at grain boundaries. International Journal of Plasticity, 2014, 61, 49-63.	8.8	56

#	Article	IF	CITATIONS
145	High Pressure Interpass Rolling of Wire + Arc Additively Manufactured Titanium Components. Advanced Materials Research, 0, 996, 694-700.	0.3	55
146	Changes in the misfit stresses in an Al/SiCp metal matrix composite under plastic strain. Acta Materialia, 2002, 50, 1031-1040.	7.9	54
147	Residual stress relief in MAG welded joints of dissimilar steels. International Journal of Pressure Vessels and Piping, 2003, 80, 705-713.	2.6	54
148	Laser Shock Peening on Zr-based Bulk Metallic Glass and Its Effect on Plasticity: Experiment and Modeling. Scientific Reports, 2015, 5, 10789.	3.3	54
149	SparseBeads data: benchmarking sparsity-regularized computed tomography. Measurement Science and Technology, 2017, 28, 124005.	2.6	54
150	A synchrotron X-ray study of a Ti/SiCf composite during in situ straining. Acta Materialia, 2001, 49, 153-163.	7.9	53
151	Study of a Crack at a Fastener Hole by Digital Image Correlation. Experimental Mechanics, 2009, 49, 551-559.	2.0	53
152	Finite element process modelling of inertia friction welding advanced nickel-based superalloy. Materials Science & Engineering A: Structural Materials: Properties, Microstructure and Processing, 2009, 513-514, 366-375.	5.6	53
153	Efficacy of active cooling for controlling residual stresses in friction stir welds. Science and Technology of Welding and Joining, 2010, 15, 156-165.	3.1	53
154	<i>In situ</i> 3D Xâ€ray microtomography study comparing auxetic and nonâ€auxetic polymeric foams under tension. Physica Status Solidi (B): Basic Research, 2011, 248, 45-51.	1.5	53
155	Reliability of Algorithms Interpreting Topological and Geometric Properties of Porous Media for Pore Network Modelling. Transport in Porous Media, 2019, 128, 271-301.	2.6	53
156	A synchrotron radiation study of transient internal strain changes during the early stages of thermal cycling in an Al / SiCw MMC. Scripta Materialia, 1996, 35, 1229-1234.	5.2	52
157	Microstructural development in Pt-aluminide coating on CMSX-4 superalloy during TMF. Surface and Coatings Technology, 1998, 107, 76-83.	4.8	52
158	In situ analysis of cracks in structural materials using synchrotron X-ray tomography and diffraction. Nuclear Instruments & Methods in Physics Research B, 2006, 246, 217-225.	1.4	52
159	The Effects of Filler Metal Transformation Temperature on Residual Stresses in a High Strength Steel Weld. Journal of Pressure Vessel Technology, Transactions of the ASME, 2009, 131, .	0.6	52
160	Neutron strain scanning using a radially collimated diffracted beam. Physica B: Condensed Matter, 2000, 292, 273-285.	2.7	51
161	The effect of thermal oxidation on polycrystalline graphite studied by X-ray tomography. Carbon, 2005, 43, 765-774.	10.3	51
162	Image stitching strategies for tomographic imaging of large objects at high resolution at synchrotron sources. Nuclear Instruments and Methods in Physics Research, Section A: Accelerators, Spectrometers, Detectors and Associated Equipment, 2009, 607, 677-684.	1.6	51

#	Article	IF	CITATIONS
163	The pulsed eddy current response to applied loading of various aluminium alloys. NDT and E International, 2010, 43, 493-500.	3.7	51
164	Investigation of interfacial properties of atmospheric plasma sprayed thermal barrier coatings with four-point bending and computed tomography technique. Surface and Coatings Technology, 2012, 206, 4922-4929.	4.8	51
165	Friction Stir Welding in HSLA-65 Steel: Part I. Influence of Weld Speed and Tool Material on Microstructural Development. Metallurgical and Materials Transactions A: Physical Metallurgy and Materials Science, 2012, 43, 2342-2355.	2.2	51
166	Measuring overload effects during fatigue crack growth in bainitic steel by synchrotron X-ray diffraction. International Journal of Fatigue, 2015, 71, 11-16.	5.7	51
167	High resolution low kV EBSD of heavily deformed and nanocrystalline Aluminium by dictionary-based indexing. Scientific Reports, 2018, 8, 10991.	3.3	51
168	Serial sectioning in the SEM for three dimensional materials science. Current Opinion in Solid State and Materials Science, 2020, 24, 100817.	11.5	51
169	Effects of Grain and Pore Size on Salt Precipitation During Evaporation from Porous Media. Transport in Porous Media, 2015, 110, 281-294.	2.6	50
170	Diffraction tomography of strain. Inverse Problems, 2015, 31, 045005.	2.0	50
171	Inertia welding nickel-based superalloy: Part II. Residual stress characterization. Metallurgical and Materials Transactions A: Physical Metallurgy and Materials Science, 2002, 33, 3227-3234.	2.2	49
172	The effect of fibre fractures in the bridging zone of fatigue cracked Ti–6Al–4V/SiC fibre composites. Acta Materialia, 2004, 52, 1423-1438.	7.9	49
173	Towards in-process x-ray CT for dimensional metrology. Measurement Science and Technology, 2016, 27, 035401.	2.6	49
174	Strain-induced reactivation of corrosion pits in austenitic stainless steel. Corrosion Science, 2017, 125, 12-19.	6.6	49
175	Overload effects on fatigue crackâ€ŧip fields under plane stress conditions: surface and bulk analysis. Fatigue and Fracture of Engineering Materials and Structures, 2013, 36, 75-84.	3.4	48
176	Influence of Surface Anomalies Following Hole Making Operations on the Fatigue Performance for a Nickel-Based Superalloy. Journal of Manufacturing Science and Engineering, Transactions of the ASME, 2014, 136, .	2.2	48
177	X-ray Computed Tomographic Investigation of the Porosity and Morphology of Plasma Electrolytic Oxidation Coatings. ACS Applied Materials & Interfaces, 2016, 8, 8801-8810.	8.0	47
178	Imaging and analysis techniques for electrical trees using X-ray computed tomography. IEEE Transactions on Dielectrics and Electrical Insulation, 2014, 21, 53-63.	2.9	47
179	Depth capabilities of neutron and synchrotron diffraction strain measurement instruments. I. The maximum feasible path length. Journal of Applied Crystallography, 2004, 37, 596-606.	4.5	46
180	Minor cutting edge–workpiece interactions in drilling of an advanced nickel-based superalloy. International Journal of Machine Tools and Manufacture, 2009, 49, 645-658.	13.4	46

#	Article	IF	CITATIONS
181	Design of weld fillers for mitigation of residual stresses in ferritic and austenitic steel welds. Science and Technology of Welding and Joining, 2011, 16, 279-284.	3.1	46
182	Micron-Scale Residual Stress Measurement by Micro-Hole Drilling and Digital Image Correlation. Experimental Mechanics, 2012, 52, 417-428.	2.0	46
183	Oxygen transport through supported Ba0.5Sr0.5Co0.8Fe0.2O3â~δ membranes. Separation and Purification Technology, 2014, 121, 60-67.	7.9	46
184	Broad ion beam serial section tomography. Ultramicroscopy, 2017, 172, 52-64.	1.9	46
185	MXene Tunable Lamellae Architectures for Supercapacitor Electrodes. ACS Applied Energy Materials, 2020, 3, 411-422.	5.1	46
186	Finite element modelling of tungsten inert gas welding of aluminium alloy 2024. Science and Technology of Welding and Joining, 2003, 8, 10-18.	3.1	45
187	Physically-based constitutive modelling of residual stress development in welding of aluminium alloy 2024. Acta Materialia, 2004, 52, 4973-4983.	7.9	45
188	Evolution of intergranular stresses during in situ straining of IF steel with different grain sizes. Materials Science & Engineering A: Structural Materials: Properties, Microstructure and Processing, 2006, 437, 26-32.	5.6	45
189	Biomechanics of Dromaeosaurid Dinosaur Claws: Application of Xâ€Ray Microtomography, Nanoindentation, and Finite Element Analysis. Anatomical Record, 2009, 292, 1397-1405.	1.4	45
190	Nanotomography for understanding materials degradation. Scripta Materialia, 2010, 63, 835-838.	5.2	45
191	Stainless steel weld metal designed to mitigate residual stresses. Science and Technology of Welding and Joining, 2009, 14, 559-565.	3.1	44
192	Friction Stir Welding of HSLA-65 Steel: Part II. The Influence of Weld Speed and Tool Material on the Residual Stress Distribution and Tool Wear. Metallurgical and Materials Transactions A: Physical Metallurgy and Materials Science, 2012, 43, 2356-2365.	2.2	44
193	Assessment of surface integrity of Ni superalloy after electrical-discharge, laser and mechanical micro-drilling processes. International Journal of Advanced Manufacturing Technology, 2015, 79, 1303-1311.	3.0	44
194	Damage evolution in braided composite tubes under torsion studied by in-situ X-ray computed tomography. Composites Science and Technology, 2020, 188, 107976.	7.8	44
195	The precision of diffraction peak location. Journal of Applied Crystallography, 2001, 34, 737-743.	4.5	43
196	Energy-input-based finite-element process modeling of inertia welding. Metallurgical and Materials Transactions B: Process Metallurgy and Materials Processing Science, 2005, 36, 513-523.	2.1	43
197	Measured residual stress distributions for low and high heat input single weld beads deposited on to SA508 steel. Materials Science and Technology, 2009, 25, 325-334.	1.6	43
198	An evaluation of the evolution of workpiece surface integrity in hole making operations for a nickel-based superalloy. Journal of Materials Processing Technology, 2012, 212, 1723-1730.	6.3	43

#	Article	IF	CITATIONS
199	Hole-Drilling Residual Stress Measurement with Artifact Correction Using Full-Field DIC. Experimental Mechanics, 2013, 53, 255-265.	2.0	43
200	In Situ Laboratory-Based Transmission X-Ray Microscopy and Tomography of Material Deformation at the Nanoscale. Experimental Mechanics, 2016, 56, 1585-1597.	2.0	43
201	X-ray micro computed tomography characterization of cellular SiC foams for their applications in chemical engineering. Materials Characterization, 2017, 123, 20-28.	4.4	43
202	Residual stress fields after FOD impact on flat and aerofoil-shaped leading edges. Mechanics of Materials, 2012, 55, 130-145.	3.2	42
203	On the three-dimensional structure of WC grains in cemented carbides. Acta Materialia, 2013, 61, 4726-4733.	7.9	42
204	Influence of wall roughness and packing density on stagnant zone formation during funnel flow discharge from a silo: An X-ray imaging study. Chemical Engineering Science, 2013, 97, 210-224.	3.8	42
205	A multi-scale correlative investigation of ductile fracture. Acta Materialia, 2017, 130, 56-68.	7.9	42
206	In situ X-ray imaging of fatigue crack growth from multiple defects in additively manufactured AlSi10Mg alloy. International Journal of Fatigue, 2022, 155, 106616.	5.7	42
207	Comparison of three different techniques for measuring the residual stresses in an electron beam-welded plate of WASPALOY. Metallurgical and Materials Transactions A: Physical Metallurgy and Materials Science, 1999, 30, 1797-1808.	2.2	41
208	Bragg Edge Determination for Accurate Lattice Parameter and Elastic Strain Measurement. Physica Status Solidi A, 2001, 185, 221-230.	1.7	41
209	SiC single fibre full-fragmentation during straining in a Ti–6Al–4V matrix studied by synchrotron X-rays. Acta Materialia, 2002, 50, 3177-3192.	7.9	41
210	A minute fossil phoretic mite recovered by phase-contrast X-ray computed tomography. Biology Letters, 2012, 8, 457-460.	2.3	41
211	Eigenstrain modelling of residual stress generated by arrays of laser shock peening shots and determination of the complete stress field using limited strain measurements. Surface and Coatings Technology, 2013, 216, 68-77.	4.8	41
212	Comparison of the Mechanical Behaviour of Standard and Auxetic Foams by Xâ€ray Computed Tomography and Digital Volume Correlation. Strain, 2013, 49, 467-482.	2.4	41
213	Crack healing behaviour of Cr 2 AlC MAX phase studied by X-ray tomography. Journal of the European Ceramic Society, 2017, 37, 441-450.	5.7	41
214	Quantifying fibre reorientation during axial compression of a composite through time-lapse X-ray imaging and individual fibre tracking. Composites Science and Technology, 2018, 168, 47-54.	7.8	41
215	Additive manufacturing assisted investment casting: A low-cost method to fabricate periodic metallic cellular lattices. Additive Manufacturing, 2020, 33, 101085.	3.0	41
216	Residual Strain Measurement by Synchrotron Diffraction. Materials Science Forum, 2002, 404-407, 1-12.	0.3	40

#	Article	IF	CITATIONS
217	Mapping Residual Stress Distributions at the Micron Scale in Amorphous Materials. Metallurgical and Materials Transactions A: Physical Metallurgy and Materials Science, 2010, 41, 1743-1751.	2.2	40
218	In-situ synchrotron X-ray tomography investigation of damage mechanism of an extruded magnesium alloy in uniaxial low-cycle fatigue with ratchetting. Acta Materialia, 2021, 211, 116881.	7.9	40
219	An investigation of the isothermal creep response of Al-based composites by neutron diffraction. Materials Science & Engineering A: Structural Materials: Properties, Microstructure and Processing, 2000, 284, 103-113.	5.6	39
220	Finite element modelling versus classic beam theory: comparing methods for stress estimation in a morphologically diverse sample of vertebrate long bones. Journal of the Royal Society Interface, 2013, 10, 20120823.	3.4	39
221	In situdetermination of stresses from time-of-flight neutron transmission spectra. Journal of Applied Crystallography, 2003, 36, 1159-1168.	4.5	38
222	Particle movement during the deep penetration of a granular material studied by X-ray microtomography. Scripta Materialia, 2006, 54, 191-196.	5.2	38
223	Improved tomographic reconstructions using adaptiveÂtime-dependent intensity normalization. Journal of Synchrotron Radiation, 2010, 17, 689-699.	2.4	38
224	Bread dough aeration dynamics during pressure step-change mixing: Studies by X-ray tomography, dough density and population balance modelling. Chemical Engineering Science, 2013, 101, 470-477.	3.8	38
225	3D imaging by serial block face scanning electron microscopy for materials science using ultramicrotomy. Ultramicroscopy, 2016, 163, 6-18.	1.9	38
226	Evolution of kink bands in a notched unidirectional carbon fibre-epoxy composite under four-point bending. Composites Science and Technology, 2019, 172, 143-152.	7.8	38
227	Damage mechanisms of coated systems under thermomechanical fatigue. Materials Science and Technology, 1999, 15, 1031-1036.	1.6	37
228	Depth capabilities of neutron and synchrotron diffraction strain measurement instruments. II. Practical implications. Journal of Applied Crystallography, 2004, 37, 607-612.	4.5	37
229	Residual stresses caused by head-on and 45° foreign object damage for a laser shock peened Ti–6Al–4V alloy aerofoil. Materials Science & Engineering A: Structural Materials: Properties, Microstructure and Processing, 2013, 560, 518-527.	5.6	37
230	A comparison of different approaches for imaging cracks in composites by X-ray microtomography. Philosophical Transactions Series A, Mathematical, Physical, and Engineering Sciences, 2016, 374, 20160037.	3.4	37
231	Micro-mechanics based damage mechanics for 3D orthogonal woven composites: Experiment and numerical modelling. Composite Structures, 2016, 156, 115-124.	5.8	37
232	Neutron diffraction study of stress-induced martensitic transformation and variant change in Fe–Pd. Acta Materialia, 2003, 51, 6453-6464.	7.9	36
233	High-resolution strain mapping in bulk samples using full-profile analysis of energy dispersive synchrotron X-ray diffraction data. Nuclear Instruments & Methods in Physics Research B, 2005, 238, 200-204.	1.4	36
234	Residual strains and microstructure development in single and sequential double sided friction stir welds in RQT-701 steel. Materials Science & Engineering A: Structural Materials: Properties, Microstructure and Processing, 2008, 492, 35-44.	5.6	36

#	Article	IF	CITATIONS
235	An analytical formula for ring artefact suppression in X-ray tomography. Applied Mathematics Letters, 2010, 23, 1489-1495.	2.7	36
236	<i>A priori</i> information in a regularized sinogram-based method for removing ring artefacts in tomography. Journal of Synchrotron Radiation, 2010, 17, 540-549.	2.4	36
237	Imaging and analysis techniques for electrical trees using X-ray computed tomography. IEEE Transactions on Dielectrics and Electrical Insulation, 2014, 21, 53-63.	2.9	36
238	Residual stresses due to foreign object damage in laser-shock peened aerofoils: Simulation and measurement. Mechanics of Materials, 2015, 82, 78-90.	3.2	36
239	Depth-profiling of residual stress and microstructure for austenitic stainless steel surface treated by cavitation, shot and laser peening. Materials Science & Engineering A: Structural Materials: Properties, Microstructure and Processing, 2021, 813, 141037.	5.6	36
240	A recurrent neural network for modelling dynamical systems. Network: Computation in Neural Systems, 1998, 9, 531-547.	3.6	35
241	Cranial anatomy ofThalassiodracon hawkinsii(Reptilia, Plesiosauria) from the Early Jurassic of Somerset, United Kingdom. Journal of Vertebrate Paleontology, 2011, 31, 562-574.	1.0	35
242	Comparison and combination of imaging techniques for three dimensional analysis of electrical trees. IEEE Transactions on Dielectrics and Electrical Insulation, 2015, 22, 709-719.	2.9	35
243	Joint image reconstruction method with correlative multi-channel prior for x-ray spectral computed tomography. Inverse Problems, 2018, 34, 064001.	2.0	35
244	The effect of shoulder coupling on the residual stress and hardness distribution in AA7050 friction stir butt welds. Materials Science & Engineering A: Structural Materials: Properties, Microstructure and Processing, 2018, 735, 218-227.	5.6	35
245	X-ray tomographic imaging of Ti/SiC composites. Journal of Microscopy, 2003, 209, 102-112.	1.8	34
246	Analysis of a prehistoric Egyptian iron bead with implications for the use and perception of meteorite iron in ancient Egypt. Meteoritics and Planetary Science, 2013, 48, 997-1006.	1.6	34
247	Determination of the constitutive relation and critical condition for the shock compression of cellular solids. Mechanics of Materials, 2016, 99, 26-36.	3.2	34
248	Time-dependent in situ measurement of atmospheric corrosion rates of duplex stainless steel wires. Npj Materials Degradation, 2018, 2, .	5.8	34
249	X-ray micro-computed tomography ( <i>μ</i> CT): an emerging opportunity in parasite imaging. Parasitology, 2018, 145, 848-854.	1.5	34
250	3D characterization of porosity in an air plasmaâ€sprayed thermal barrier coating and its effect on thermal conductivity. Journal of the American Ceramic Society, 2018, 101, 2482-2492.	3.8	34
251	The variation of the unstrained lattice parameter in an AA7010 friction stir weld. Acta Materialia, 2007, 55, 4111-4120.	7.9	33
252	Mechanical Tensioning of High-Strength Aluminum Alloy Friction Stir Welds. Metallurgical and Materials Transactions A: Physical Metallurgy and Materials Science, 2008, 39, 3246-3259.	2.2	33

#	Article	IF	CITATIONS
253	4-D imaging of sub-second dynamics in pore-scale processes using real-time synchrotron X-ray tomography. Solid Earth, 2016, 7, 1059-1073.	2.8	33
254	Response and representation of ductile damage under varying shock loading conditions in tantalum. Journal of Applied Physics, 2016, 119, .	2.5	33
255	Influence of Tow Architecture on Compaction and Nesting in Textile Preforms. Applied Composite Materials, 2017, 24, 337-350.	2.5	33
256	Multiscale correlative tomography: an investigation of creep cavitation in 316 stainless steel. Scientific Reports, 2017, 7, 7332.	3.3	33
257	Digital element simulation of aligned tows during compaction validated by computed tomography (CT). International Journal of Solids and Structures, 2018, 154, 78-87.	2.7	33
258	Investigation of residual stress distribution and texture evolution in AA7050 stationary shoulder friction stir welded joints. Materials Science & Engineering A: Structural Materials: Properties, Microstructure and Processing, 2018, 712, 531-538.	5.6	33
259	Measurements of fibre bridging during fatigue crack growth in Ti/SiC fibre metal matrix composites. Acta Materialia, 2003, 51, 1045-1057.	7.9	32
260	Crack opening displacements during fatigue crack growth in Ti–SiC fibre metal matrix composites by X-ray tomography. Materials Science and Technology, 2006, 22, 1052-1058.	1.6	32
261	Bainite orientation in plastically deformed austenite. International Journal of Materials Research, 2009, 100, 40-45.	0.3	32
262	Fatigue crack growth and load redistribution in Ti/SiC composites observed in situ. Acta Materialia, 2009, 57, 590-599.	7.9	32
263	Noncontact evaluation of the dependency of electrical conductivity on stress for various Al alloys as a function of plastic deformation and annealing. Journal of Applied Physics, 2010, 108, 024909.	2.5	32
264	Microstructural analysis of TRISO particles using multi-scale X-ray computed tomography. Journal of Nuclear Materials, 2015, 461, 29-36.	2.7	32
265	Characterization of the three-dimensional structure of a metallic foam during compressive deformation. Journal of Microscopy, 2006, 223, 150-158.	1.8	31
266	Prediction of residual stress distributions for single weld beads deposited on to SA508 steel including phase transformation effects. Materials Science and Technology, 2010, 26, 940-949.	1.6	31
267	Fibre bundles in the human extensor carpi ulnaris tendon are arranged in a spiral. Journal of Hand Surgery: European Volume, 2012, 37, 550-554.	1.0	31
268	X-ray Tomographic Imaging of Tensile Deformation Modes of Electrospun Biodegradable Polyester Fibers. Frontiers in Materials, 2017, 4, .	2.4	31
269	The heterogenous distribution of white etching matter (WEM) around subsurface cracks in bearing steels. Acta Materialia, 2019, 174, 300-309.	7.9	31
270	Texture of poled tetragonal PZT detected by synchrotron X-ray diffraction and micromechanics analysis. Materials Science & Engineering A: Structural Materials: Properties, Microstructure and Processing, 2005, 409, 206-210.	5.6	30

#	Article	IF	CITATIONS
271	Evaluation of the interfacial shear strength and residual stress of TiAlN coating on ZIRLOâ,,¢ fuel cladding using a modified shear-lag model approach. Journal of Nuclear Materials, 2015, 466, 718-727.	2.7	30
272	Weld zone and residual stress development in AA7050 stationary shoulder friction stir T-joint weld. Journal of Materials Processing Technology, 2019, 263, 256-265.	6.3	30
273	A conformable high temperature nitride coating for Ti alloys. Acta Materialia, 2020, 189, 274-283.	7.9	30
274	Tomographic Reconstruction of Neopterous Carboniferous Insect Nymphs. PLoS ONE, 2012, 7, e45779.	2.5	30
275	4D-CT reconstruction with unified spatial-temporal patch-based regularization. Inverse Problems and Imaging, 2015, 9, 447-467.	1.1	30
276	A new stroboscopic neutron diffraction method for monitoring materials subjected to cyclic loads: Thermal cycling of metal matrix composites. Scripta Materialia, 1996, 35, 717-720.	5.2	29
277	Prediction of hardness minimum locations during natural aging in an aluminum alloy 6061-T6 friction stir weld. Journal of Materials Science, 2009, 44, 6302-6309.	3.7	29
278	Effects of superimposed electric field and porosity on the hydrostatic pressure-induced rhombohedral to orthorhombic martensitic phase transformation in PZT 95/5 ceramics. Acta Materialia, 2010, 58, 6584-6591.	7.9	29
279	Computed tomography recovers data from historical amber: an example from huntsman spiders. Die Naturwissenschaften, 2011, 98, 519-527.	1.6	29
280	Work hardening induced by martensite during transformation-induced plasticity in plain carbon steel. Acta Materialia, 2012, 60, 6931-6939.	7.9	29
281	Assessment of machining performance using the wear map approach in micro-drilling. International Journal of Advanced Manufacturing Technology, 2012, 59, 119-126.	3.0	29
282	TomoPhantom, a software package to generate 2D–4D analytical phantoms for CT image reconstruction algorithm benchmarks. SoftwareX, 2018, 7, 150-155.	2.6	29
283	Comparing Xe <sup>+</sup> pFIB and Ga <sup>+</sup> FIB for TEM sample preparation of Al alloys: Minimising FIBâ€induced artefacts. Journal of Microscopy, 2021, 282, 101-112.	1.8	29
284	Core Imaging Library - Part I: a versatile Python framework for tomographic imaging. Philosophical Transactions Series A, Mathematical, Physical, and Engineering Sciences, 2021, 379, 20200192.	3.4	29
285	Effects of tooling on the residual stress distribution in an inertia weld. Materials Science & Engineering A: Structural Materials: Properties, Microstructure and Processing, 2003, 356, 405-413.	5.6	28
286	Stress relaxation of shot-peened UDIMET 720Li under solely elevated-temperature exposure and under isothermal fatigue. Metallurgical and Materials Transactions A: Physical Metallurgy and Materials Science, 2005, 36, 3041-3053.	2.2	28
287	Mapping Residual Stress Profiles at the Micron Scale Using FIB Micro-Hole Drilling. Applied Mechanics and Materials, 0, 24-25, 267-272.	0.2	28
288	Nonintrusive estimation of anisotropic stiffness maps of heterogeneous steel welds for the improvement of ultrasonic array inspection. IEEE Transactions on Ultrasonics, Ferroelectrics, and Frequency Control, 2015, 62, 1530-1543.	3.0	28

#	Article	IF	CITATIONS
289	The influence of electrodeposited Ni-Co alloy coating microstructure on CO2 corrosion resistance on X65 steel. Corrosion Science, 2020, 167, 108485.	6.6	28
290	Interpreting pathologies in extant and extinct archosaurs using micro-CT. PeerJ, 2015, 3, e1130.	2.0	28
291	The determination of the residual strains and stresses in a tungsten inert gas welded sheet of IN718 superalloy using neutron diffraction. Journal of Strain Analysis for Engineering Design, 2000, 35, 247-259.	1.8	27
292	Evolution of crack-bridging and crack-tip driving force during the growth of a fatigue crack in a Ti/SiC composite. Proceedings of the Royal Society A: Mathematical, Physical and Engineering Sciences, 2012, 468, 2722-2743.	2.1	27
293	Submicron-scale depth profiling of residual stress in amorphous materials by incremental focused ion beam slotting. Acta Materialia, 2012, 60, 2337-2349.	7.9	27
294	Piezomorphic Materials. Macromolecular Materials and Engineering, 2013, 298, 318-327.	3.6	27
295	Anisotropic crack propagation and deformation in dentin observed by four-dimensional X-ray nano-computed tomography. Acta Biomaterialia, 2019, 96, 400-411.	8.3	27
296	The deformation of discontinuously reinforced MMCs—II. The elastic response. Acta Metallurgica Et Materialia, 1994, 42, 3437-3442.	1.8	26
297	Measurement and modelling of residual stresses in a TIG weld. Applied Physics A: Materials Science and Processing, 2002, 74, s1421-s1423.	2.3	26
298	Residual Stress Measurements in Single and Multi-Pass Groove Weld Specimens Using Neutron Diffraction and the Contour Method. Materials Science Forum, 2006, 524-525, 671-676.	0.3	26
299	Revisiting the blocking force test on ferroelectric ceramics using high energy x-ray diffraction. Journal of Applied Physics, 2015, 117, 174104.	2.5	26
300	4D visualisation of <i>in situ</i> nano-compression of Li-ion cathode materials to mimic early stage calendering. Materials Horizons, 2019, 6, 612-617.	12.2	26
301	A three-dimensional mechanistic study of the drivers of classical twin nucleation and variant selection in Mg alloys: A mesoscale modelling and experimental study. International Journal of Plasticity, 2021, 143, 103027.	8.8	26
302	Congestive Heart Failure Leads to Prolongation of the PR Interval and Atrioventricular Junction Enlargement and Ion Channel Remodelling in the Rabbit. PLoS ONE, 2015, 10, e0141452.	2.5	26
303	Prediction of damage evolution in forged aluminium metal matrix composites using a neural network approach. Journal of Materials Processing Technology, 1998, 80-81, 507-512.	6.3	25
304	A new method of performance verification for x-ray computed tomography measurements. Measurement Science and Technology, 2014, 25, 065401.	2.6	25
305	Characterisation of overloads in fatigue by 2D strain mapping at the surface and in the bulk. Fatigue and Fracture of Engineering Materials and Structures, 2016, 39, 1040-1048.	3.4	25
306	The application of 3D imaging techniques, simulation and diffusion experiments to explore transport properties in porous oxygen transport membrane support materials. Solid State Ionics, 2016, 288, 315-321.	2.7	25

#	Article	IF	CITATIONS
307	Thermo – mechanical properties of SPS produced self-healing thermal barrier coatings containing pure and alloyed MoSi2 particles. Journal of the European Ceramic Society, 2018, 38, 4268-4275.	5.7	25
308	Laminography in the lab: imaging planar objects using a conventional x-ray CT scanner. Measurement Science and Technology, 2019, 30, 035401.	2.6	25
309	4D imaging of void nucleation, growth, and coalescence from large and small inclusions in steel under tensile deformation. Journal of Materials Science and Technology, 2022, 123, 168-176.	10.7	25
310	Mapping of unstressed lattice parameters using pulsed neutron transmission diffraction. Journal of Applied Crystallography, 2002, 35, 497-504.	4.5	24
311	Macro and intergranular stress responses of austenitic stainless steel to 90° strain path changes. Materials Science & Engineering A: Structural Materials: Properties, Microstructure and Processing, 2012, 546, 263-271.	5.6	24
312	The anatomy and grain pattern in forks of hazel (Corylus avellana L.) and other tree species. Trees - Structure and Function, 2014, 28, 1437-1448.	1.9	24
313	Multiscale 3D analysis of creep cavities in AISI type 316 stainless steel. Materials Science and Technology, 2015, 31, 522-534.	1.6	24
314	Residual Stresses in Linear Friction Welded IMI550. Journal of Neutron Research, 2004, 12, 165-173.	1.1	23
315	<i>In Situ </i> Monitoring of Weld Transformations to Control Weld Residual Stresses. Materials Science Forum, 0, 571-572, 393-398.	0.3	23
316	Characterization of microplasticity in TiAl-based alloys. Acta Materialia, 2009, 57, 1357-1366.	7.9	23
317	Real-time acquisition of fatigue crack images for monitoring crack-tip stress intensity variations within fatigue cycles. Journal of Strain Analysis for Engineering Design, 2009, 44, 149-158.	1.8	23
318	A multiscale model for reversible ferroelectric behaviour of polycrystalline ceramics. Mechanics of Materials, 2014, 71, 85-100.	3.2	23
319	The role of crack branching in stress corrosion cracking of aluminium alloys. Corrosion Reviews, 2015, 33, 443-454.	2.0	23
320	Application of a Quasi In Situ Experimental Approach to Estimate 3-D Pitting Corrosion Kinetics in Stainless Steel. Journal of the Electrochemical Society, 2016, 163, C745-C751.	2.9	23
321	How to fragment peralkaline rhyolites: Observations on pumice using combined multi-scale 2D and 3D imaging. Journal of Volcanology and Geothermal Research, 2017, 336, 179-191.	2.1	23
322	Quantifying fatigue overload retardation mechanisms by energy dispersive X-ray diffraction. Journal of the Mechanics and Physics of Solids, 2019, 124, 392-410.	4.8	23
323	An examination of the mean stress contribution to the Bauschinger effect by neutron diffraction. Materials Science & Engineering A: Structural Materials: Properties, Microstructure and Processing, 1995, 197, 215-221.	5.6	22
324	The influence of temperature on microstructural damage during uniaxial compression of aluminium matrix composites. Scripta Metallurgica Et Materialia, 1995, 33, 323-329.	1.0	22

#	Article	IF	CITATIONS
325	The extent of relaxation of weld residual stresses on cutting out cross-weld test-pieces. Powder Diffraction, 2009, 24, S31-S36.	0.2	22
326	Fault location and diagnosis in a medium voltage EPR power cable. IEEE Transactions on Dielectrics and Electrical Insulation, 2013, 20, 10-18.	2.9	22
327	High Spatial Resolution Evaluation of Residual Stresses in Shot Peened Specimens Containing Sharp and Blunt Notches by Micro-hole Drilling, Micro-slot Cutting and Micro-X-ray Diffraction Methods. Experimental Mechanics, 2016, 56, 1449-1463.	2.0	22
328	New software protocols for enabling laboratory based temporal CT. Review of Scientific Instruments, 2018, 89, 093702.	1.3	22
329	Tracking capsule activation and crack healing in a microcapsule-based self-healing polymer. Scientific Reports, 2019, 9, 17773.	3.3	22
330	3D characterisation of dry powder inhaler formulations: Developing X-ray micro computed tomography approaches. European Journal of Pharmaceutics and Biopharmaceutics, 2020, 151, 32-44.	4.3	22
331	Core Imaging Library - Part II: multichannel reconstruction for dynamic and spectral tomography. Philosophical Transactions Series A, Mathematical, Physical, and Engineering Sciences, 2021, 379, 20200193.	3.4	22
332	Evolution of fibre deflection leading to kink-band formation in unidirectional glass fibre/epoxy composite under axial compression. Composites Science and Technology, 2021, 213, 108929.	7.8	22
333	Considerations in the use of yield asymmetries for the analysis of internal stresses in metal matrix composites. Materials Science & Engineering A: Structural Materials: Properties, Microstructure and Processing, 1992, 159, 51-63.	5.6	21
334	Neutron Diffraction Study of Extruded Magnesium during Cyclic and Elevated Temperature Loading. Materials Science Forum, 2005, 490-491, 257-262.	0.3	21
335	Scientific Review: First Impressions of SALSA: The New Engineering Instrument at ILL. Neutron News, 2006, 17, 28-32.	0.2	21
336	Mapping the evolution of density in 3D of thermally oxidised graphite for nuclear applications. Scripta Materialia, 2006, 54, 829-834.	5.2	21
337	A ring artifact suppression algorithm based on a priori information. Applied Physics Letters, 2009, 95, 071113.	3.3	21
338	Thermal Relaxation of Residual Stresses in Nickel-Based Superalloy Inertia Friction Welds. Metallurgical and Materials Transactions A: Physical Metallurgy and Materials Science, 2011, 42, 2301-2311.	2.2	21
339	Dependence of dielectric behavior in BiFeO3 ceramics on intrinsic defects. Journal of Alloys and Compounds, 2012, 541, 94-98.	5.5	21
340	Characterising the Integrity of Machined Surfaces in a Powder Nickel Alloy used in Aircraft Engines. Procedia CIRP, 2014, 13, 411-416.	1.9	21
341	Late-stage fatigue damage in a 3D orthogonal non-crimp woven composite: An experimental and numerical study. Composites Part A: Applied Science and Manufacturing, 2015, 79, 155-163.	7.6	21
342	Influence of embedded MoSi2 particles on the high temperature thermal conductivity of SPS produced yttria-stabilised zirconia model thermal barrier coatings. Surface and Coatings Technology, 2016, 308, 31-39.	4.8	21

#	Article	IF	CITATIONS
343	The effect of the weld fusion zone shape on residual stress in submerged arc welding. International Journal of Advanced Manufacturing Technology, 2017, 90, 3451-3464.	3.0	21
344	Redistribution of carbon caused by butterfly defects in bearing steels. Acta Materialia, 2020, 183, 390-397.	7.9	21
345	The effect of grain size on the fatigue overload behaviour of nickel. Materials and Design, 2020, 189, 108526.	7.0	21
346	Generation of high-fidelity random fields from micro CT images and phase field-based mesoscale fracture modelling of concrete. Engineering Fracture Mechanics, 2021, 249, 107762.	4.3	21
347	Iterative estimates of internal stresses in short-fibre metal matrix composites. Philosophical Magazine A: Physics of Condensed Matter, Structure, Defects and Mechanical Properties, 1992, 65, 1217-1233.	0.6	20
348	Interfacial shear strength of Ti/SiC fibre composites measured by synchrotron strain measurement. Composites Part A: Applied Science and Manufacturing, 2002, 33, 1381-1385.	7.6	20
349	Imaging and strain mapping fibre by fibre in the vicinity of a fatigue crack in a Ti/SiC fibre composite. Materials Science and Technology, 2005, 21, 27-34.	1.6	20
350	A plasticity model for powder compaction processes incorporating particle deformation and rearrangement. International Journal of Solids and Structures, 2008, 45, 2056-2076.	2.7	20
351	Strain Measurement by Digital Image Correlation. Strain, 2008, 44, 421-422.	2.4	20
352	Soft body impact resistance of composite foam core sandwich panels with unidirectional corrugated and tubular reinforcements. International Journal of Impact Engineering, 2019, 132, 103320.	5.0	20
353	Tracking the calcium-magnesium-alumino-silicate (CMAS) infiltration into an air-plasma spray thermal barrier coating using X-ray imaging. Scripta Materialia, 2020, 176, 94-98.	5.2	20
354	Coupled Broad Ion Beam–Scanning Electron Microscopy (BIB–SEM) for polishing and three dimensional (3D) serial section tomography (SST). Ultramicroscopy, 2020, 214, 112989.	1.9	20
355	Multiscale image-based modelling of damage and fracture in carbon fibre reinforced polymer composites. Composites Science and Technology, 2020, 198, 108243.	7.8	20
356	Micromechanics of failure of aluminide coated single crystal Ni superalloy under thermomechanical fatigue. Scripta Materialia, 1997, 37, 815-820.	5.2	19
357	Image Processing Issues in Digital Strain Mapping. , 2002, , .		19
358	The Appropriateness of Residual Stress Length Scales in Structural Integrity. Journal of Neutron Research, 2004, 12, 81-91.	1.1	19
359	The role of surface condition, residual stress and microstructure on pre-yield cracking in Ti44Al8Nb1B. Intermetallics, 2004, 12, 281-287.	3.9	19
360	Characterization of laser peening residual stresses in Al 7075 by synchrotron diffraction and the contour method. Journal of Neutron Research, 2007, 15, 147-154.	1.1	19

#	Article	IF	CITATIONS
361	Spatially Resolved Materials Property Data From a Uniaxial Cross-Weld Tensile Test. Journal of Pressure Vessel Technology, Transactions of the ASME, 2009, 131, .	0.6	19
362	Suppression of ring artefacts when tomographing anisotropically attenuating samples. Journal of Synchrotron Radiation, 2011, 18, 427-435.	2.4	19
363	3D Crackâ€ŧip Microscopy: Illuminating Microâ€&cale Effects on Crackâ€Ţip Behavior. Advanced Engineering Materials, 2011, 13, 1096-1100.	3.5	19
364	A Graphical Processing Unit–Based Parallel Implementation of Multiplicative Algebraic Reconstruction Technique Algorithm for Limited View Tomography. Research in Nondestructive Evaluation, 2013, 24, 211-222.	1.1	19
365	Revealing the three dimensional internal structure of aluminium alloys. Surface and Interface Analysis, 2013, 45, 1536-1542.	1.8	19
366	Phase transition modeling of polytetrafluoroethylene during Taylor impact. Journal of Applied Physics, 2014, 116, .	2.5	19
367	A novel technique to incorporate structural prior information into multi-modal tomographic reconstruction. Inverse Problems, 2014, 30, 065004.	2.0	19
368	Employing temporal self-similarity across the entire time domain in computed tomography reconstruction. Philosophical Transactions Series A, Mathematical, Physical, and Engineering Sciences, 2015, 373, 20140389.	3.4	19
369	Correlative multiscale tomography of biological materials. MRS Bulletin, 2016, 41, 549-556.	3.5	19
370	An evaluation of diffraction peak profile analysis (DPPA) methods to study plastically deformed metals. Materials and Design, 2016, 111, 331-343.	7.0	19
371	Hot dwell-fatigue behaviour of additively manufactured AlSi10Mg alloy: Relaxation, cyclic softening and fracture mechanisms. International Journal of Fatigue, 2021, 151, 106408.	5.7	19
372	Ancient Ephemeroptera–Collembola Symbiosis Fossilized in Amber Predicts Contemporary Phoretic Associations. PLoS ONE, 2012, 7, e47651.	2.5	19
373	Elastic strains around cracked cold-expanded fastener holes measured using the synchrotron X-ray diffraction technique. Journal of Strain Analysis for Engineering Design, 2004, 39, 459-469.	1.8	18
374	Pattern decomposition and quantitative-phase analysis in pulsed neutron transmission. Physica B: Condensed Matter, 2004, 350, 159-161.	2.7	18
375	Transformation Temperatures and Welding Residual Stresses in Ferritic Steels. , 2007, , 949.		18
376	Shakedown of deep cold rolling residual stresses in titanium alloys. Journal Physics D: Applied Physics, 2008, 41, 174005.	2.8	18
377	Interfacial shear strength behaviour of Ti/SiC metal matrix composites at room and elevated temperature. Acta Materialia, 2010, 58, 6090-6103.	7.9	18
378	Three-dimensional observation and image-based modelling of thermal strains in polycrystalline alumina. Acta Materialia, 2013, 61, 7521-7533.	7.9	18

#	Article	IF	CITATIONS
379	The Role of Crossâ€Sectional Geometry, Curvature, and Limb Posture in Maintaining Equal Safety Factors: A Computed Tomography Study. Anatomical Record, 2013, 296, 395-413.	1.4	18
380	Novel implementations of relaxation methods for measuring residual stresses at the micron scale. Journal of Strain Analysis for Engineering Design, 2015, 50, 412-425.	1.8	18
381	Timeâ€lapse labâ€based xâ€ray nanoâ€CT study of corrosion damage. Journal of Microscopy, 2017, 267, 98-106.	1.8	18
382	Time-lapse 3D imaging of calcite precipitation in a microporous column. Geochimica Et Cosmochimica Acta, 2018, 222, 156-170.	3.9	18
383	Residual stress control of multipass welds using low transformation temperature fillers. Materials Science and Technology, 2018, 34, 519-528.	1.6	18
384	Fatigue crack nuclei in austempered ductile cast iron. Fatigue and Fracture of Engineering Materials and Structures, 2002, 25, 635-648.	3.4	17
385	Measurement and Prediction of the Residual Stress Field Generated by Side-Punching. Journal of Engineering Materials and Technology, Transactions of the ASME, 2006, 128, 451-459.	1.4	17
386	Micromechanics of domain switching in rhombohedral PZT ceramics. Ceramics International, 2008, 34, 679-683.	4.8	17
387	A new species of anapid spider (Araneae: Araneoidea, Anapidae) in Eocene Baltic amber, imaged using phase contrast X-ray computed micro-tomography. Zootaxa, 2011, 2742, 60.	0.5	17
388	Synchrotron analysis of toughness anomalies in nanostructured bainite. Acta Materialia, 2016, 105, 52-58.	7.9	17
389	MicroCT imaging reveals differential 3D micro-scale remodelling of the murine aorta in ageing and Marfan syndrome. Theranostics, 2018, 8, 6038-6052.	10.0	17
390	CCPi-Regularisation toolkit for computed tomographic image reconstruction with proximal splitting algorithms. SoftwareX, 2019, 9, 317-323.	2.6	17
391	Following the effect of braid architecture on performance and damage of carbon fibre/epoxy composite tubes during torsional straining. Composites Science and Technology, 2020, 200, 108451.	7.8	17
392	Realization of 3D epoxy resin/Ti <sub>3</sub> C <sub>2</sub> T <sub>x</sub> MXene aerogel composites for low-voltage electrothermal heating. 2D Materials, 2021, 8, 025022.	4.4	17
393	Macro-, meso- and microstructural characterization of metallic lattice structures manufactured by additive manufacturing assisted investment casting. Scientific Reports, 2021, 11, 4974.	3.3	17
394	Internal stress induced debonding in a zirconia-reinforced 6061 aluminium alloy composite. Materials Science & Engineering A: Structural Materials: Properties, Microstructure and Processing, 1993, 171, 1-11.	5.6	16
395	Separation of measured fatigue crack stress fields in a metal matrix composite material. Acta Materialia, 1999, 47, 585-593.	7.9	16
396	Residual Stress Field in a Friction Stir Welded Aluminium Extrusion. Materials Science Forum, 2000, 347-349, 678-683.	0.3	16

#	Article	IF	CITATIONS
397	Finite element modelling of frictional bridging during fatigue crack growth in fibre-reinforced metal matrix composites. Computational Materials Science, 2002, 25, 166-173.	3.0	16
398	Intergranular Stress Evolution in Titanium Studied by Neutron Diffraction and Self-consistent Modelling. Journal of Neutron Research, 2004, 12, 33-37.	1.1	16
399	Mixed Mode (K <sub>l</sub> +K <sub>ll</sub> ) Stress Intensity Factor Measurement by Electronic Speckle Pattern Interferometry and Image Correlation. Applied Mechanics and Materials, 2004, 1-2, 107-112.	0.2	16
400	A deconvolution method for the reconstruction of underlying profiles measured using large sampling volumes. Journal of Applied Crystallography, 2006, 39, 410-424.	4.5	16
401	SALSA: Advances in Residual Stress Measurement at ILL. Materials Science Forum, 2006, 524-525, 217-222.	0.3	16
402	Using augmented reality to promote an understanding of materials science to school children. , 2008, , .		16
403	A Comparison of Residual Stress Development in Inertia Friction Welded Fine Grain and Coarse Grain Nickel-Base Superalloy. Metallurgical and Materials Transactions A: Physical Metallurgy and Materials Science, 2011, 42, 4056-4063.	2.2	16
404	MRI measurements of vessel calibre in tumour xenografts: Comparison with vascular corrosion casting. Microvascular Research, 2012, 84, 323-329.	2.5	16
405	Fibre bridging during high temperature fatigue crack growth in Ti/SiC composites. Acta Materialia, 2012, 60, 958-971.	7.9	16
406	Back Stress Work Hardening Confirmed by Bauschinger Effect in a TRIP Steel Using Bending Tests. ISIJ International, 2014, 54, 1715-1718.	1.4	16
407	Micro-CT evaluation of the effectiveness of the combined use of rotary and hand instrumentation in removal of Resilon. Dental Materials Journal, 2014, 33, 1-6.	1.8	16
408	Use of Particle Tracking to Determine Optimal Release Dates and Locations for Rehabilitated Neonate Sea Turtles. Frontiers in Marine Science, 2017, 4, .	2.5	16
409	Time-Lapse Helical X-ray Computed Tomography (CT) Study of Tensile Fatigue Damage Formation in Composites for Wind Turbine Blades. Materials, 2018, 11, 2340.	2.9	16
410	Measuring the Particle Packing of <scp>l</scp> -Glutamic Acid Crystals through X-ray Computed Tomography for Understanding Powder Flow and Consolidation Behavior. Crystal Growth and Design, 2020, 20, 4252-4263.	3.0	16
411	Tracking polycrystal evolution non-destructively in 3D by laboratory X-ray diffraction contrast tomography. Materials Characterization, 2021, 172, 110814.	4.4	16
412	The determination of the profile of macrostress and thermal mismatch stress through an Al/SiCp composite plate from the average residual strains measured in each phase. Physica B: Condensed Matter, 1995, 213-214, 790-792.	2.7	15
413	A method for the 3-D quantification of bridging ligaments during crack propagation. Scripta Materialia, 2011, 65, 131-134.	5.2	15
414	Combining X-ray microtomography and three-dimensional digital volume correlation to track microstructure evolution during sintering of copper powder. Journal of Strain Analysis for Engineering Design, 2014, 49, 257-269.	1.8	15

#	Article	IF	CITATIONS
415	Fatigue Behavior of Shot Peened Notched Specimens: Effect of the Residual Stress Field Ahead of the Notch Root. Procedia Engineering, 2015, 109, 80-88.	1.2	15
416	Xe+ Plasma FIB: 3D Microstructures from Nanometers to Hundreds of Micrometers. Microscopy Today, 2016, 24, 32-39.	0.3	15
417	X-ray Tomography Characterisation of Lattice Structures Processed by Selective Electron Beam Melting. Metals, 2017, 7, 300.	2.3	15
418	Time-lapse three-dimensional imaging of crack propagation in beetle cuticle. Acta Biomaterialia, 2019, 86, 109-116.	8.3	15
419	Correction of artefacts associated with large area EBSD. Ultramicroscopy, 2021, 226, 113315.	1.9	15
420	Fine equiaxed zone induced softening and failure behavior of 7050 aluminum alloy hybrid laser welds. Materials Science & Engineering A: Structural Materials: Properties, Microstructure and Processing, 2021, 821, 141597.	5.6	15
421	Neutron Strain Measurement of Internal Strain in Metal and Ceramic Matrix Composites. Key Engineering Materials, 1995, 108-110, 291-314.	0.4	14
422	In situ monitoring of thermally cycled metal matrix composites by neutron diffraction and laser extensometry. Applied Composite Materials, 1997, 4, 375-392.	2.5	14
423	Micromechanical analysis of internal stress development during single-fibre fragmentation testing of Ti/SiCf. Acta Materialia, 2002, 50, 2477-2490.	7.9	14
424	Process–microstructure–property correlations in Al–Li AA2199 friction stir welds. Science and Technology of Welding and Joining, 2010, 15, 522-527.	3.1	14
425	The production and characterization of topologically and mechanically gradient open-cell thermoplastic foams. Smart Materials and Structures, 2014, 23, 055016.	3.5	14
426	Characterisation and modelling of defect formation in direct-chill cast AZ80 alloy. Materials Characterization, 2015, 104, 116-123.	4.4	14
427	Comparison of grain to grain orientation and stiffness mapping by spatially resolved acoustic spectroscopy and EBSD. Journal of Microscopy, 2017, 267, 89-97.	1.8	14
428	Model-based iterative reconstruction using higher-order regularization of dynamic synchrotron data. Measurement Science and Technology, 2017, 28, 094004.	2.6	14
429	Determination of local residual stress in an air plasma spray thermal barrier coating (APS-TBC) by microscale ring coring using a picosecond laser. Scripta Materialia, 2019, 167, 126-130.	5.2	14
430	Experimental steering of electron microscopy studies using prior X-ray computed tomography. Ultramicroscopy, 2019, 201, 58-67.	1.9	14
431	Various TEM methods for the study of metal matrix composites. Journal of Microscopy, 1988, 151, 159-169.	1.8	13
432	Regularization methods for inverse problems in x-ray tomography. Proceedings of SPIE, 2010, , .	0.8	13

#	Article	IF	CITATIONS
433	Effects of stop–start features on residual stresses in a multipass austenitic stainless steel weld. International Journal of Pressure Vessels and Piping, 2012, 89, 9-18.	2.6	13
434	The influence of shock-loading path on the spallation response of Ta. Journal of Physics: Conference Series, 2014, 500, 112031.	0.4	13
435	Temporal sparsity exploiting nonlocal regularization for 4D computed tomography reconstruction. Journal of X-Ray Science and Technology, 2016, 24, 207-219.	1.0	13
436	The effect of anisotropic microstructure on the crack growth and fatigue overload behaviour of ultrafine-grained nickel. Acta Materialia, 2020, 184, 225-240.	7.9	13
437	An in-situ method for protecting internal cracks/pores from ion beam damage and reducing curtaining for TEM sample preparation using FIB. Ultramicroscopy, 2020, 219, 113135.	1.9	13
438	Environmentally induced crack (EIC) initiation, propagation, and failure: A 3D in-situ time-lapse study of AA5083 H131. Corrosion Science, 2020, 174, 108834.	6.6	13
439	In-situ X-ray microtomography study of the movement of a granular material within a die. International Journal of Materials Research, 2012, 103, 162-169.	0.3	13
440	Steady-state creep of a composite. Mechanics of Materials, 2001, 33, 493-498.	3.2	12
441	In-situneutron diffraction study of the rhombohedral to orthorhombic phase transformation in lead zirconate titanate ceramics produced by uniaxial compression. Philosophical Magazine Letters, 2007, 87, 41-52.	1.2	12
442	Elastic and plastic strain effects on eddy current response of aluminium alloys. Nondestructive Testing and Evaluation, 2013, 28, 300-312.	2.1	12
443	Investigation of the elastic/crystallographic anisotropy of welds for improved ultrasonic inspections. Materials Characterization, 2014, 98, 47-53.	4.4	12
444	Peak broadening anisotropy in deformed face-centred cubic and hexagonal close-packed alloys. Journal of Applied Crystallography, 2014, 47, 1535-1551.	4.5	12
445	Obtaining the J-integral by diffraction-based crack-field strain mapping. Procedia Structural Integrity, 2016, 2, 2519-2526.	0.8	12
446	A Novel Tomographic Reconstruction Method Based on the Robust Student's t Function For Suppressing Data Outliers. IEEE Transactions on Computational Imaging, 2017, 3, 682-693.	4.4	12
447	Effect of hydration and crack orientation on crack-tip strain, crack opening displacement and crack-tip shielding in elephant dentin. Dental Materials, 2018, 34, 1041-1053.	3.5	12
448	Initiation and short crack growth behaviour of environmentally induced cracks in AA5083 H131 investigated across time and length scales. Corrosion Reviews, 2019, 37, 469-481.	2.0	12
449	X-ray Micro-Computed Tomography: An Emerging Technology to Analyze Vascular Calcification in Animal Models. International Journal of Molecular Sciences, 2020, 21, 4538.	4.1	12
450	Characterisation of cuticular inflation development and ultrastructure in Trichuris muris using correlative X-ray computed tomography and electron microscopy. Scientific Reports, 2020, 10, 5846.	3.3	12

#	Article	IF	CITATIONS
451	Size segregation of irregular granular materials captured by time-resolved 3D imaging. Scientific Reports, 2021, 11, 8352.	3.3	12
452	Comments on "The strength differential and bauschinger effects in SiC-Al composites― Materials Science & Engineering A: Structural Materials: Properties, Microstructure and Processing, 1989, 108, 281-284.	5.6	11
453	Examination of tensile/compressive loading asymmetries in aluminium based metal matrix composites using finite element method. Materials Science and Technology, 1995, 11, 228-235.	1.6	11
454	Plastic bending of a residually stressed beam. International Journal of Solids and Structures, 1997, 34, 1985-2002.	2.7	11
455	Accelerated learning using Gaussian process models to predict static recrystallization in an Al-Mg alloy. Modelling and Simulation in Materials Science and Engineering, 2000, 8, 687-706.	2.0	11
456	A neutron diffraction study of creep and damage occurrence in an A359/SiC composite. Materials Science & Engineering A: Structural Materials: Properties, Microstructure and Processing, 2002, 333, 232-238.	5.6	11
457	Neutron diffraction study of the deformation behaviour of deformation processed copper–chromium composites. Materials Science & Engineering A: Structural Materials: Properties, Microstructure and Processing, 2003, 348, 208-216.	5.6	11
458	Residual Stress Driven Creep Cracking in Type 316 Stainless Steel. Journal of Neutron Research, 2004, 12, 45-49.	1.1	11
459	Domain switching in rhombohedral PZT ceramics under electrical and mechanical loading. Materials Science and Technology, 2008, 24, 927-933.	1.6	11
460	Shear cracking in an Al powder compact studied by X-ray microtomography. Materials Science & Engineering A: Structural Materials: Properties, Microstructure and Processing, 2009, 508, 64-70.	5.6	11
461	Non-contact characterization of hybrid aluminium/carbon-fibre-reinforced plastic sheets using multi-frequency eddy-current sensors. Measurement Science and Technology, 2010, 21, 105708.	2.6	11
462	Optimal lodine Staining of Cardiac Tissue for X-Ray Computed Tomography. PLoS ONE, 2014, 9, e105552.	2.5	11
463	Time-lapse imaging of particle invasion and deposition in porous media using in situ X-ray radiography. Journal of Petroleum Science and Engineering, 2019, 177, 384-391.	4.2	11
464	Exploiting Confinement to Study the Crystallization Pathway of Calcium Sulfate. Advanced Functional Materials, 2021, 31, 2107312.	14.9	11
465	A recurrent neural network for modelling dynamical systems. Network: Computation in Neural Systems, 1998, 9, 531-547.	3.6	11
466	Effect of thermal residual stresses on fatigue crack opening and propagation behavior in an Al/SiC p metal matrix composite. Metallurgical and Materials Transactions A: Physical Metallurgy and Materials Science, 1995, 26, 3191-3198.	2.2	10
467	Numerical prediction of the development of particle stress in the forging of aluminium metal matrix composites. Journal of Materials Processing Technology, 1996, 60, 711-718.	6.3	10
468	Diagnosing Engineering Problems with Neutrons. MRS Bulletin, 1999, 24, 17-23.	3.5	10

#	Article	IF	CITATIONS
469	The Effect of Fatigue on Residual Peening Stresses in Aerospace Components. Materials Science Forum, 2005, 490-491, 340-345.	0.3	10
470	Application of a micromechanics model to the overall properties of heterogeneous graphite. Journal of Nuclear Materials, 2008, 381, 124-128.	2.7	10
471	Microstructure and properties of hot isostatically pressed powder and extruded Ti25V15Cr2AlO·2C. Materials Science and Technology, 2011, 27, 1241-1248.	1.6	10
472	Microstructure of <i> In Situ</i> Mg Metal Matrix Composites Based on Silica Nanoparticles. Solid State Phenomena, 0, 191, 189-198.	0.3	10
473	Fourier basis for the engineering assessment of cracks in residual stress fields. Engineering Fracture Mechanics, 2012, 91, 37-50.	4.3	10
474	Imaging cracks in hostile regimes. Nature Materials, 2013, 12, 7-9.	27.5	10
475	Identification of crystalline elastic anisotropy in PZT ceramics from in-situ blocking stress measurements. Journal of Applied Physics, 2014, 115, 174102.	2.5	10
476	Behavior of 316L stainless steel containing corrosion pits under cyclic loading. Materials and Corrosion - Werkstoffe Und Korrosion, 2019, 70, 2009-2019.	1.5	10
477	In situ through-thickness analysis of crack tip fields with synchrotron X-ray diffraction. International Journal of Fatigue, 2019, 127, 500-508.	5.7	10
478	Multi-modal plasma focused ion beam serial section tomography of an organic paint coating. Ultramicroscopy, 2019, 197, 1-10.	1.9	10
479	pyCM: An open-source computational framework for residual stress analysis employing the Contour Method. SoftwareX, 2020, 11, 100458.	2.6	10
480	Crystalline phase discriminating neutron tomography using advanced reconstruction methods. Journal Physics D: Applied Physics, 2021, 54, 325502.	2.8	10
481	Compaction, nesting and image based permeability analysis of multi-layer dry preforms by computed tomography (CT). Composite Structures, 2021, 263, 113676.	5.8	10
482	High-resolution, in-situ, tomographic observations of stress corrosion cracking. , 2008, , 439-447.		10
483	Characterisation of y' across inertia friction welded Alloy 720Li. , 2004, , .		10
484	Enhanced hyperspectral tomography for bioimaging by spatiospectral reconstruction. Scientific Reports, 2021, 11, 20818.	3.3	10
485	Tailoring the Microstructure of Lamellar Ti <sub>3</sub> C <sub>2</sub> T <sub><i>x</i></sub> MXene Aerogel by Compressive Straining. ACS Nano, 2022, 16, 1896-1908.	14.6	10
486	Synchrotron X-ray study of micromechanics of Ti/SiCfcomposites with fibres containing defects introduced by laser drilling. Materials Science and Technology, 2002, 18, 1497-1503.	1.6	9

#	Article	IF	CITATIONS
487	SALSA: Strain Analyser for Large and Small Scale Engineering Applications. Journal of Neutron Research, 2003, 11, 235-239.	1.1	9
488	Orientation dependence of martensite variants during loading of Fe–Pd shape memory alloy. Scripta Materialia, 2005, 53, 609-612.	5.2	9
489	Comparison using neutron diffraction of martensitic transformation in Fe–Mn–Si shape memory alloys with and without VN precipitates. Materials Science and Technology, 2008, 24, 902-907.	1.6	9
490	Inertia friction welds between nickel superalloy components: Analysis of residual stress by eigenstrain distributions. Journal of Strain Analysis for Engineering Design, 2009, 44, 159-170.	1.8	9
491	Application of anisotropic inclusion theory to the energy evaluation for the matrix channel deformation and rafting geometry of γâ°`γ′ Ni superalloys. Materials Science & Engineering A: Structural Materials: Properties, Microstructure and Processing, 2009, 505, 41-47.	5.6	9
492	A multiscale modelling analysis of the contribution of crystalline elastic anisotropy to intergranular stresses in ferroelectric materials. Journal Physics D: Applied Physics, 2014, 47, 325303.	2.8	9
493	Effect of sugar on bread dough aeration during mixing. Journal of Food Engineering, 2015, 150, 9-18.	5.2	9
494	Quantifying the metallurgical response of a nuclear steel to welding thermal cycles. Materials Science and Technology, 2016, 32, 1517-1532.	1.6	9
495	Synchrotron X-ray diffraction based method for stress intensity factor evaluation in the bulk of materials. Theoretical and Applied Fracture Mechanics, 2018, 98, 72-77.	4.7	9
496	On the Application of Xe+ Plasma FIB for Micro-fabrication of Small-scale Tensile Specimens. Experimental Mechanics, 2019, 59, 1113-1125.	2.0	9
497	2D mapping of plane stress crack-tip fields following an overload. Frattura Ed Integrita Strutturale, 2015, 9, 151-158.	0.9	9
498	Use of the frozen-stress photoelastic method to explore load partitioning in short-fibre composites. Materials Science & Engineering A: Structural Materials: Properties, Microstructure and Processing, 1991, 135, 173-178.	5.6	8
499	Stress Induced Martensitic Transformation Studied by Neutron Diffraction. Materials Science Forum, 2002, 404-407, 489-494.	0.3	8
500	Effects of Texture and Anisotropy on Intergranular Stress Development in Zirconium. Materials Science Forum, 2005, 495-497, 1553-1558.	0.3	8
501	Geometry Effects when Controlling Residual Stresses in Friction Stir Welds by Mechanical Tensioning. Materials Science Forum, 2006, 524-525, 71-76.	0.3	8
502	Three-dimensional imaging of materials by microtomography. Materials Science and Technology, 2006, 22, 1009-1010.	1.6	8
503	The Use of Diffraction to Study Fatigue Crack Tip Mechanics. Materials Science Forum, 2010, 652, 216-221.	0.3	8
504	Synchrotron Strain Mapping of the Residual Strain Distribution around Foreign Object Damage in Laser Shock Peened Ti-6AL-4V Alloy. Materials Science Forum, 2010, 652, 19-24.	0.3	8

#	Article	IF	CITATIONS
505	Assessment of the Deformation of Low Density Polymeric Auxetic Foams by X-Ray Tomography and Digital Volume Correlation. Applied Mechanics and Materials, 0, 70, 93-98.	0.2	8
506	Post-processing techniques for making reliable measurements from curve-skeletons. Computers in Biology and Medicine, 2016, 72, 120-131.	7.0	8
507	X-ray microtomography as a tool for investigating the petrological context of Precambrian cellular remains. Geological Society Special Publication, 2017, 448, 33-56.	1.3	8
508	Industrial Gear Oils: Tribological Performance and Subsurface Changes. Tribology Letters, 2018, 66, 65.	2.6	8
509	In Situ Study of the Stress Relaxation During Aging of Nickel-Base Superalloy Forgings. Metallurgical and Materials Transactions A: Physical Metallurgy and Materials Science, 2019, 50, 3555-3565.	2.2	8
510	Crystallographic tomography and molecular modelling of structured organic polycrystalline powders. CrystEngComm, 2021, 23, 2520-2531.	2.6	8
511	The Effect of Clustering on Damage Formation in Particulate Reinforced MMCs Deformed in Compression. Key Engineering Materials, 1996, 127-131, 937-944.	0.4	7
512	Measurement and prediction of residual stresses in a titanium metal matrix composite ring. Journal of Neutron Research, 2001, 9, 373-379.	1.1	7
513	Computational assessment of the influence of load ratio on fatigue crack growth in fibre-reinforced metal matrix composites. International Journal of Fatigue, 2002, 24, 1205-1211.	5.7	7
514	Multi-scale finite-element modelling of fatigue-crack growth in TiAl intermetallic matrix TiNb and Nb platelet composites. Acta Materialia, 2002, 50, 1453-1466.	7.9	7
515	Near Surface Residual Stress Determination of Laser Shock Peening by Neutron Diffraction. Journal of Neutron Research, 2003, 11, 229-233.	1.1	7
516	An evaluation of recurrent neural network modelling for the prediction of damage evolution during forming. Journal of Materials Processing Technology, 2005, 170, 551-562.	6.3	7
517	A verified model of laser direct metal deposition using an analytical enthalpy balance method. , 2007, , .		7
518	The shock response, simulation and microstructural determination of a model composite material. Journal of Materials Science, 2007, 42, 9671-9678.	3.7	7
519	Comparison of methods to determine variations in unstrained unit cell parameter across welds. Journal of Strain Analysis for Engineering Design, 2011, 46, 651-662.	1.8	7
520	A novel approach for imaging of electrical trees. , 2012, , .		7
521	The Oldest Fossil Pirate Spider (Araneae: Mimetidae), in Uppermost Eocene Indian Amber, Imaged Using X-ray Computed Tomography. Arachnology, 2012, 15, 299-302.	0.4	7
522	A new species of Craspedisia (Araneae: Theridiidae) in Miocene Dominican amber, imaged using X-ray computed tomography. Paleontological Journal, 2012, 46, 583-588.	0.5	7

#	Article	IF	CITATIONS
523	Effects of Cooling Rates on Glass Formation and Magnetic Behavior for the Fe73.0C7.0Si3.3B5.0P8.7Mo3.0 Bulk Metallic Glass. Metallurgical and Materials Transactions A: Physical Metallurgy and Materials Science, 2013, 44, 2004-2009.	2.2	7
524	Saurichthys (Pisces, Actinopterygii) teeth from the Lower Triassic of Spitsbergen, with comments on their stable isotope composition (δ13C and δ18O) and Xâ^'ray microtomography. Polish Polar Research, 2013, 34, 23-38.	0.9	7
525	Three dimensional characterisation of electrical trees. , 2013, , .		7
526	Multimodal Image Reconstruction Using Supplementary Structural Information in Total Variation Regularization. Sensing and Imaging, 2014, 15, 97.	1.5	7
527	Degradation of metallic materials studied by correlative tomography. IOP Conference Series: Materials Science and Engineering, 2017, 219, 012001.	0.6	7
528	Industrial Gear Oils: Influence of Bulk Oil Temperature and Contact Pressure on Tribological Performance and Subsurface Changes. Tribology Letters, 2020, 68, 1.	2.6	7
529	Damage accumulation during high temperature fatigue of Ti/SiCf metal matrix composites under different stress amplitudes. Acta Materialia, 2021, 213, 116976.	7.9	7
530	Ultrafine grain structures formed by thermomechanical processing of spray cast Al–Li alloys. Materials Science and Technology, 1999, 15, 605-615.	1.6	6
531	Monitoring elastic strain and damage by neutron and synchrotron X-ray beams. Materials Science and Technology, 2001, 17, 759-765.	1.6	6
532	Elevated temperature tensile properties and failure of a copper-chromium in situ composite. Journal of Materials Science, 2003, 38, 3437-3447.	3.7	6
533	Observation and quantitative analysis of damage caused by creep in an A1 A359/SiC P composite. Materials Science & Engineering A: Structural Materials: Properties, Microstructure and Processing, 2003, 342, 201-206.	5.6	6
534	The Engineering Body Scanner Concept. Journal of Neutron Research, 2003, 11, 247-253.	1.1	6
535	Study of Residual Stresses Introduced by Laser Shock Peening in Wide Chord Fan Blades by Neutron and Synchrotron Diffraction. Journal of Neutron Research, 2004, 12, 207-211.	1.1	6
536	Micromechanics of stress-induced martensitic transformation. Materials Science & Engineering A: Structural Materials: Properties, Microstructure and Processing, 2004, 378, 479-483.	5.6	6
537	Residual Stress Mapping in Railway Rails. Materials Science Forum, 2005, 490-491, 165-170.	0.3	6
538	Characterisation of Residual Stresses in Machined Surfaces of a High Strength Nickel-Base Superalloy. Materials Science Forum, 2006, 524-525, 587-592.	0.3	6
539	Non-Contact Characterisation of Carbon-Fibre-Reinforced Plastics (CFRP) Using Multi-frequency Eddy Current Sensors. Conference Record - IEEE Instrumentation and Measurement Technology Conference, 2007, , .	0.0	6
540	Robotic sample manipulation for stress and texture determination on neutron and synchrotron X-ray diffractometers. Nuclear Instruments and Methods in Physics Research, Section A: Accelerators, Spectrometers, Detectors and Associated Equipment, 2008, 584, 428-435.	1.6	6

#	Article	IF	CITATIONS
541	Predicting the onset of rafting of γ′ precipitates by channel deformation in a Ni superalloy. Philosophical Magazine, 2010, 90, 585-597.	1.6	6
542	Modelling the Interpass Temperature Effect on Residual Stress in Low Transformation Temperature Stainless Steel Welds. , 2011, , .		6
543	Techniques for electrical tree imaging. , 2012, , .		6
544	A new method for quantifying anisotropic martensitic transformation strains accumulated during constrained cooling. Materials Science & Engineering A: Structural Materials: Properties, Microstructure and Processing, 2014, 611, 354-361.	5.6	6
545	Full-field energy-dispersive powder diffraction imaging using laboratory X-rays. Journal of Applied Crystallography, 2015, 48, 269-272.	4.5	6
546	Characterisation of an Advanced Nickel Based Superalloy Post Cold Work by Swaging. Metals, 2016, 6, 54.	2.3	6
547	Residual Stress: Measurement by Diffraction. , 2016, , .		6
548	Dynamic damage in carbon-fibre composites. Philosophical Transactions Series A, Mathematical, Physical, and Engineering Sciences, 2016, 374, 20160018.	3.4	6
549	Determination of residual stress at weld interruptions by neutron diffraction. Zeitschrift Für Kristallographie, Supplement, 2008, 2008, 231-243.	0.5	6
550	Damage evolution in freeze cast metal/ceramic composites exhibiting lamellar microstructures. Frattura Ed Integrita Strutturale, 2015, 9, 134-142.	0.9	6
551	Forging of â€~H' sections from aluminium metal matrix composite bars, modelled using the finite element method. Journal of Materials Processing Technology, 1994, 45, 421-428.	6.3	5
552	A look ahead in residual stress analysis: the strain imager at the ILL. , 2002, 4785, 64.		5
553	Mechanical energy criterion for stress-induced martensitic transformation. Scripta Materialia, 2003, 49, 1013-1019.	5.2	5
554	Residual Stress Prediction for the Inertia Welding Process. Journal of Neutron Research, 2004, 12, 21-25.	1.1	5
555	Implications of interface friction for crack growth in fibre-reinforced metal matrix composites by three-dimensional finite element modelling. International Journal of Fracture, 2004, 125, 281-305.	2.2	5
556	Neutron diffraction study of stress-induced martensitic transformation and variant change in Fe–Pd shape memory alloy. Materials Science & Engineering A: Structural Materials: Properties, Microstructure and Processing, 2004, 378, 328-332.	5.6	5
557	Residual Stress Measurements Revealing Weld Bead Start and Stop Effects in Single and Multi-Pass Weld-Runs. , 2005, , 853.		5
558	Synchrotron X-ray measurement and finite element analysis of residual strain in tungsten inert gas welded aluminum alloy 2024. Metallurgical and Materials Transactions A: Physical Metallurgy and Materials Science, 2006, 37, 3629-3637.	2.2	5

#	Article	IF	CITATIONS
559	FE Modelling of Mechanical Tensioning for Controlling Residual Stresses in Friction Stir Welds. Materials Science Forum, 0, 539-543, 4025-4030.	0.3	5
560	Stress distributions in multilayer laser deposited Waspaloy parts measured using neutron diffraction. , 2007, , .		5
561	Comparison of the X-ray performance of small pixel CdTe and CZT detectors. , 2010, , .		5
562	Depth and Lateral Variation of Machining-Induced Residual Stress for a Nickel Base Superalloy. Materials Science Forum, 2011, 681, 332-339.	0.3	5
563	Assessment of Thread-Cutting Strategies to Enable Damage-Tolerant Surfaces on an Advanced Ni-Based Aerospace Superalloy. Proceedings of the Institution of Mechanical Engineers, Part B: Journal of Engineering Manufacture, 2011, 225, 12-24.	2.4	5
564	Three dimensional imaging of electrical trees in micro and nano-filled epoxy resin. , 2014, , .		5
565	X-ray microtomography study of the spallation response in Ta-W. Journal of Physics: Conference Series, 2014, 500, 112045.	0.4	5
566	Geochemical Evidence of the Seasonality, Affinity and Pigmenation of Solenopora jurassica. PLoS ONE, 2015, 10, e0138305.	2.5	5
567	Comparison and combination of imaging techniques for three dimensional analysis of electrical trees. IEEE Transactions on Dielectrics and Electrical Insulation, 2015, 22, 709-719.	2.9	5
568	Microstructural degradation of Electron Beam-Physical Vapour Deposition Thermal Barrier Coating during thermal cycling tracked by X-ray micro-computed tomography. Scripta Materialia, 2018, 152, 79-83.	5.2	5
569	MAR-M-247 creep assessment through a modified theta projection model. Materialia, 2019, 7, 100392.	2.7	5
570	Assessing the efficacy of tomographic reconstruction methods through physical quantification techniques. Measurement Science and Technology, 2021, 32, 075404.	2.6	5
571	Comparative Analysis of Shot-Peened Residual Stresses Using Micro-Hole Drilling, Micro-Slot Cutting, X-ray Diffraction Methods and Finite-Element Modelling. Conference Proceedings of the Society for Experimental Mechanics, 2016, , 215-223.	0.5	5
572	Frictional behaviour of Al359/SiC/20p composite under isothermal and non-isothermal hot-working conditions as a function of surface roughness. Journal of Materials Processing Technology, 1997, 72, 195-200.	6.3	4
573	Measurement and Prediction of Residual Stresses in Aluminium Friction Stir Welds. Journal of Neutron Research, 2003, 11, 267-272.	1.1	4
574	The effect of process parameters on residual stresses within an inconel 718 part produced by the direct laser deposition process. , 2005, , .		4
575	Measuring and Predicting the Effects of Residual Stresses on Crack Propagation. Materials Science Forum, 2006, 524-525, 77-82.	0.3	4
576	Relaxation of Residual Stresses in and around Mechanical Fasteners Due to Fatigue Loading. Materials Science Forum, 2006, 524-525, 153-158.	0.3	4

#	Article	IF	CITATIONS
577	Residual stresses in and around electromagnetically installed rivets measured using synchrotron and neutron diffraction. Journal of Neutron Research, 2007, 15, 215-223.	1.1	4
578	Coplanar waveguide scanning microwave profiler. , 2007, , .		4
579	An anisotropic enhanced thermal conductivity approach for modelling laser melt pools. , 2007, , .		4
580	An examination of phase retrieval algorithms as applied to phase contrast tomography using laboratory sources. , 2010, , .		4
581	Imaging fossilised spiders in amber using lab-based phase contrast x-ray tomography. Proceedings of SPIE, 2010, , .	0.8	4
582	Spallation response of Ti-6Al-4V: Rear surface velocimetry and X-ray tomography. AIP Conference Proceedings, 2012, , .	0.4	4
583	Sparsity seeking total generalized variation for undersampled tomographic reconstruction. , 2016, , .		4
584	Correlative Tomography for Additive Manufacturing of Biomedical Implants. Microscopy and Microanalysis, 2017, 23, 342-343.	0.4	4
585	Time-Lapse Correlative 3D Imaging Applied to the Corrosion Study of AZ31ÂMg Alloy in a Saline Environment. , 2018, , 165-177.		4
586	Plasma FIB Spin Milling for Large Volume Serial Sectioning Tomography. Microscopy and Microanalysis, 2019, 25, 350-351.	0.4	4
587	Rich multi-dimensional correlative imaging. IOP Conference Series: Materials Science and Engineering, 2019, 580, 012014.	0.6	4
588	Role of SiC and Si3N4 reinforcing particles in the tribological performance of graphite-based composites. Wear, 2020, 456-457, 203399.	3.1	4
589	The 3-dimensional anatomy of the North-Western Marsupial Mole (Notoryctes caurinus Thomas 1920) using computed tomography, X-ray and magnetic resonance imaging. Records of the Western Australian Museum, 2003, 22, 1.	0.8	4
590	Improved thermal conductivity of graphite though infiltration with SiC and Si3N4 inclusions. Journal of the European Ceramic Society, 2022, 42, 1877-1883.	5.7	4
591	Investigation of Residual Stress Induced Crack Closure and its Effects on Fatigue in Metal Matrix Composites. Key Engineering Materials, 1996, 127-131, 1183-1190.	0.4	3
592	Title is missing!. Applied Composite Materials, 1997, 4, 375-393.	2.5	3
593	In situ phase strain monitoring during isothermal creep of metal matrix composites. Physica B: Condensed Matter, 1997, 234-236, 972-973.	2.7	3
594	Measurement of cavitation damage in isothermally crept Al/SiCp composites using small-angle neutron scattering. Physica B: Condensed Matter, 1997, 234-236, 1022-1023.	2.7	3

#	Article	IF	CITATIONS
595	Model-neutron diffraction strain measurement comparisons for steady state creep of metal matrix composites. Materials Science & Engineering A: Structural Materials: Properties, Microstructure and Processing, 2000, 285, 408-411.	5.6	3
596	The expected uncertainty of diffraction-peak location. Applied Physics A: Materials Science and Processing, 2002, 74, s112-s114.	2.3	3
597	Mechanical Property Mapping Using Image Correlation and Electronic Speckle Interferometry. Applied Mechanics and Materials, 2004, 1-2, 147-152.	0.2	3
598	An Analysis of Lattice Strain due to Disclination Dipole Walls in Fe-Pd Martensite. Journal of Neutron Research, 2004, 12, 39-44.	1.1	3
599	Mapping Residual-Stress Distributions in a Laser-Peened Vit-105 Bulk-Metallic Glass Using the Focused-Ion-Beam Micro-Slitting Method. Materials Research Society Symposia Proceedings, 2011, 1300, 1.	0.1	3
600	Microstructural Characterization of SOFC Electrodes: Observations and Simulations. ECS Transactions, 2011, 35, 1367-1377.	0.5	3
601	The effect of minimum dwell cycles on the environmental and fatigue response of RR1000. MATEC Web of Conferences, 2014, 14, 04003.	0.2	3
602	In Situ Synchrotron Studies of Reversible and Irreversible Non-elastic Strain in a Two-Phase TiAl Alloy. Metallurgical and Materials Transactions A: Physical Metallurgy and Materials Science, 2014, 45, 607-618.	2.2	3
603	Large volume 3D characterization by plasma FIB DualBeam microscopy. Microscopy and Microanalysis, 2015, 21, 2003-2004.	0.4	3
604	On compression and damage evolution in two thermoplastics. Proceedings of the Royal Society A: Mathematical, Physical and Engineering Sciences, 2017, 473, 20160495.	2.1	3
605	On the compression of aluminium foam structures under shock. AIP Conference Proceedings, 2017, , .	0.4	3
606	On the high-rate failure of carbon fibre composites. AIP Conference Proceedings, 2017, , .	0.4	3
607	Developments in Large Volume 3D Analysis via P-FIB: EBSD & EDS. Microscopy and Microanalysis, 2017, 23, 284-285.	0.4	3
608	3D Imaging of Indentation Damage in Bone. Materials, 2018, 11, 2533.	2.9	3
609	7.6 Computed Tomography of Composites. , 2018, , 101-118.		3
610	Investigation of Cracking in Additively Manufactured IN718 by Correlative Tomography. Microscopy and Microanalysis, 2018, 24, 366-367.	0.4	3
611	Advances in Multi-Beam and Multi-Ion FIB-SEM for 3D Correlative Microscopy. Microscopy and Microanalysis, 2019, 25, 870-871.	0.4	3
612	Morphological variability in the mucosal attachment site of Trichuris muris revealed by X-ray microcomputed tomography. International Journal for Parasitology, 2021, 51, 797-807.	3.1	3

#	Article	IF	CITATIONS
613	X-ray computed tomographic and focused ion beam/electron microscopic investigation of coating defects in niobium-coated copper superconducting radio-frequency cavities. Materials Chemistry and Physics, 2021, 273, 125062.	4.0	3
614	Micro-CT Evaluation of Voids in the Filling Material of Single-Rooted Teeth Obturated with Different Techniques. Journal of Research and Practice in Dentistry, 0, , 1-10.	0.0	3
615	Characterisation of the crack tip plastic zone in fatigue via synchrotron Xâ€ray diffraction. Fatigue and Fracture of Engineering Materials and Structures, 2022, 45, 2086-2098.	3.4	3
616	Plastic deformation. , 1993, , 71-116.		2
617	The sin2 Ï^-method in pulsed neutron transmission. Journal of Neutron Research, 2001, 9, 289-294.	1.1	2
618	Creep of a composite with a diffusional creeping matrix. Materials Science & Engineering A: Structural Materials: Properties, Microstructure and Processing, 2002, 335, 320-323.	5.6	2
619	Dynamic Analysis of Residual Stress Introduced by Laser Peening. Materials Science Forum, 2006, 524-525, 135-140.	0.3	2
620	Focus on martensitic transformations. Materials Science and Technology, 2008, 24, 883-883.	1.6	2
621	Non-contact characterisation of Carbon Fibre Reinforced Plastics in hybrid aluminium / CFRP sheets using multi-frequency eddy current sensors. , 2009, , .		2
622	Application of anisotropic inclusion theory to the deformation of Ni based single crystal superalloys: Stress–strain curves determination. Mechanics of Materials, 2010, 42, 237-247.	3.2	2
623	Investigation of Transformation Induced Plasticity and Residual Stress Analysis in Stainless Steel Welds. , 2010, , .		2
624	Porting the AVS/Express scientific visualization software to Cray XT4. Philosophical Transactions Series A, Mathematical, Physical, and Engineering Sciences, 2011, 369, 3398-3412.	3.4	2
625	Measurement of Residual Stresses in Surface Treated Stainless Steel Groove Welds. Materials Science Forum, 2011, 681, 49-54.	0.3	2
626	On the Stress Development in SA508 Autogenous Weld. Materials Science Forum, 0, 783-786, 2123-2128.	0.3	2
627	A Xe + Plasma FIB Milling and Lift-out Approach for Site-specific Preparation of Large Volume Blocks for 3D-EBSD. Microscopy and Microanalysis, 2016, 22, 838-839.	0.4	2
628	Evolution of Residual Stress in Tensile Armour Wires of Flexible Pipes During Pipe Manufacture. , 2017, , .		2
629	Automated 3D Block Preparation Procedure for Focused Ion Beam 3D Analyses. Microscopy and Microanalysis, 2017, 23, 286-287.	0.4	2
630	Three dimensional imaging of electrical trees in multiple stages. , 2017, , .		2

#	Article	IF	CITATIONS
631	High temperature low cycle fatigue characterization of equiaxed MAR-M-247. International Journal of Fatigue, 2019, 123, 225-237.	5.7	2
632	Novel Methods for Recording Stress-Strain Curves in Proton Irradiated Material. Scientific Reports, 2020, 10, 5353.	3.3	2
633	Nanoscale orientation mapping made easy: a new sample preparation workflow for rapid, large-area TKD analysis. Microscopy and Microanalysis, 2021, 27, 1596-1598.	0.4	2
634	Correlative Tomography - Bridging the length-scales through correlative X-ray and Electron Imaging. Microscopy and Microanalysis, 2021, 27, 932-933.	0.4	2
635	Modelling the Residual Stress Field Ahead of the Notch Root in Shot Peened V-Notched Samples. Conference Proceedings of the Society for Experimental Mechanics, 2016, , 249-261.	0.5	2
636	In Situ Investigation and Image-Based Modelling of Aluminium Foam Compression Using Micro X-Ray Computed Tomography. Augmented Vision and Reality, 2014, , 189-197.	0.2	2
637	FE Modelling of Mechanical Tensioning for Controlling Residual Stresses in Friction Stir Welds. Materials Science Forum, 0, , 4025-4030.	0.3	2
638	A study of the progression of damage in an axially loaded Branta leucopsis femur using X-ray computed tomography and digital image correlation. PeerJ, 2017, 5, e3416.	2.0	2
639	Simulation of Rotational Welding Operations. , 2010, , 432-442.		2
640	Theory and Modelling of Composites. , 1992, , 421-437.		2
641	Elastic and Thermoelastic Properties of Brittle Matrix Composites. , 2000, , 25-45.		1
642	The d0-distribution in Al-2024 friction stir welds. Journal of Neutron Research, 2001, 9, 345-350.	1.1	1
643	Monitoring Elastic Strain and Damage by Neutron and Synchrotron Beams. Advanced Engineering Materials, 2001, 3, 453-460.	3.5	1
644	NEUTRON SCATTERING: Enhanced: The Case for Neutron Sources. Science, 2002, 298, 543-543.	12.6	1
645	Neural Network Modeling for the Prediction of Texture Evolution of Hot Deformed Aluminum Alloys. Journal of Materials Engineering and Performance, 2003, 12, 623-628.	2.5	1
646	Diode laser metal deposition: The effect of pulsed beam parameters on superalloy microstructure and deposit morphology. , 2006, , .		1
647	The Shock Response, Simulation and Microstructural Determination of an Inert Simulant. AIP Conference Proceedings, 2006, , .	0.4	1
648	Residual Stress Analysis Around Foreign Object Damage Using Synchrotron Diffraction. Materials Science Forum, 2006, 524-525, 291-296.	0.3	1

#	Article	IF	CITATIONS
649	A Comparison of Strain Measurements on an Inertia Friction Weld Using the ENGIN-X and SALSA Neutron Strain Mapping Instruments. Materials Science Forum, 2006, 524-525, 393-398.	0.3	1
650	Scanning Microwave Profiler. , 2006, , .		1
651	Mixed Mode (I+II) Stress Intensity Factor Measurement Using Image Correlation. , 2006, , 427-428.		1
652	Residual Stress Measurements in Autogenous SA508 Steel Welds. , 2008, , .		1
653	A Comparison of Residual Stresses in Single-Pass and Multipass SA508 Steel Welds. , 2010, , .		1
654	3D inspection of fabrication and degradation processes from X-ray (micro) tomography images using a hole closing algorithm. , 2010, , .		1
655	<i>In-Situ</i> Observation and Modelling of Intergranular Cracking in Polycrystalline Alumina. Key Engineering Materials, 0, 465, 560-563.	0.4	1
656	X-Ray Microtomography for 3D Microstructure Characterization of Magnesium Matrix Composite Reinforced with Glassy Carbon Particles. Solid State Phenomena, 2011, 176, 119-126.	0.3	1
657	Three-dimensional imaging of inhomogeneous lithologies using X-ray computed tomography: characterization of drill core from the Borrowdale Volcanic Group. Mineralogical Magazine, 2012, 76, 2931-2938.	1.4	1
658	Study of overload effects in bainitic steel by synchrotron X-ray diffraction. Frattura Ed Integrita Strutturale, 2013, 7, 153-160.	0.9	1
659	Three-dimensional characterisation and simulation of deformation and damage during Taylor impact in PTFE. Journal of Physics: Conference Series, 2014, 500, 182035.	0.4	1
660	Measurement of Residual Stress Shakedown in Pressure/Tensile Armour Wires of Flexible Pipes by Neutron Diffraction. , 2015, , .		1
661	X-ray microscopy for in situ characterization of 3D nanostructural evolution in the laboratory. , 2015, , .		1
662	Improved Low Cycle Fatigue Analysis for Ni-Based Turbine Nozzles. , 2018, , .		1
663	Estimation of the plastic zone in fatigue through the thickness based on synchrotron diffraction data. Procedia Structural Integrity, 2019, 17, 872-877.	0.8	1
664	Plasma FIB Spin Milling for 3D Residual Stress Measurements. Microscopy and Microanalysis, 2019, 25, 882-883.	0.4	1
665	Observing the evolution of fatigue damage and associated strain fields in a correlative, multiscale 3D time-lapse study of quasi-unidirectional glass fibre composites. IOP Conference Series: Materials Science and Engineering, 2020, 942, 012039.	0.6	1
666	Unlocking secrets of inhalation blends through X-ray Computed Tomography and Microscopy. Microscopy and Microanalysis, 2021, 27, 292-295.	0.4	1

#	Article	IF	CITATIONS
667	Residual Stresses in Microelectronics. , 2001, , 8142-8148.		1
668	Spatially Resolved Materials Property Data From a Cross-Weld Tensile Test. , 2007, , .		1
669	SALSA: Advances in Residual Stress Measurement at ILL. Materials Science Forum, 0, , 217-222.	0.3	1
670	Characterisation of Residual Stresses in Machined Surfaces of a High Strength Nickel-Base Superalloy. Materials Science Forum, 0, , 587-592.	0.3	1
671	Dynamic Analysis of Residual Stress Introduced by Laser Peening. Materials Science Forum, 0, , 135-140.	0.3	1
672	Surface Decoration for Improving the Accuracy of Displacement Measurements by Digital Image Correlation in SEM. Conference Proceedings of the Society for Experimental Mechanics, 2013, , 217-224.	0.5	1
673	Characterizing the effects of elevated temperature on the air void pore structure of advanced gas-cooled reactor pressure vessel concrete using x-ray computed tomography. EPJ Web of Conferences, 2013, 56, 04003.	0.3	1
674	A recurrent neural network for modelling dynamical systems. Network: Computation in Neural Systems, 1998, 9, 531-47.	3.6	1
675	Recovering the second moment of the strain distribution from neutron Bragg edge data. Applied Physics Letters, 2022, 120, 164102.	3.3	1
676	Reinforcement phase stability during ageing of an aluminium alloy/yttria-stabilised zirconia composite. Scripta Metallurgica Et Materialia, 1993, 29, 1189-1194.	1.0	0
677	Composites, Physical Properties of. , 2001, , 1402-1411.		0
678	Synchrotron strain scanning on BM16 at the ESRF. Journal of Neutron Research, 2001, 9, 93-98.	1.1	0
679	Synchrotron Micro-tomography and Strain Mapping on a Fatigue Cracked Ti/SiC Fibre Composite. Journal of Neutron Research, 2004, 12, 195-199.	1.1	0
680	Shakedown During Fatigue of Residual Stresses Introduced by Different Mechanical Surface Treatments. , 2006, , 203.		0
681	Residual Stress Measurement Within a Single Pass Groove Weld Specimen Utilising Neutron Diffraction and the Contour Method. , 2006, , 907.		0
682	High-Rate Compaction of Aluminium Alloy Foams. AIP Conference Proceedings, 2006, , .	0.4	0
683	Identification of Weld Residual Stress Length Scales for Fracture Assessment. , 2006, , 1327-1328.		0
684	Neutron diffraction characterisation of thermomechanical behaviour of Fe-Mn-Si shape memory alloy. Journal of Neutron Research, 2007, 15, 179-184.	1.1	0

#	Article	IF	CITATIONS
685	A Comparison of Measurement and Modelling of Plastically Induced Residual Stresses in a 316H and a Weld 347 Stainless Steel. , 2007, , .		0
686	Process inspections and the OECD GLP Principles. Quality Assurance Journal, 2007, 11, 105-107.	0.1	0
687	Fatigue Crack Monitoring Using Image Correlation. Key Engineering Materials, 0, 385-387, 341-344.	0.4	0
688	Annealing Models in Welding Simulation: Conservative and Non-Conservative Residual Stress Distributions. , 2010, , .		0
689	The Deformation of Face-Centred-Cubic Metals Measured by Diffraction Peak Profile Analysis. Materials Science Forum, 0, 652, 139-142.	0.3	0
690	Modelling the effects of phase transformations on welding stress and distortion. , 2011, , 78-100.		0
691	Crack Tip Behaviour in Residual Stress Field: Finite Element Modelling and Neutron Diffraction Measurements. , 2011, , .		0
692	A REGION OF INTEREST COMPUTED TOMOGRAPHY TECHNIQUE FOR INSPECTION OF CFRP LAMINATES. , 2011, , .		0
693	Characterization of Cement Microstructure for the Immobilization of Nuclear Waste Using Advanced Imaging Methods. Materials Research Society Symposia Proceedings, 2012, 1475, 521.	0.1	0
694	The Influence of Geometry on Residual Stress Around Repair Welds. , 2013, , .		0
695	On the Thermo-Mechanical Behaviour of SA508 Grade 4 Ferritic Steel. , 2014, , .		0
696	Development of Simplified Empirical Phase Transformation Model for Use in Welding Residual Stress Simulations. , 2014, , .		0
697	Strain-rate sensitivity of foam materials: A numerical study using 3D image-based finite element model. EPJ Web of Conferences, 2015, 94, 04022.	0.3	0
698	An in situ Method for Preserving Buried Voids and Cracks During TEM Sample Preparation using FIB. Microscopy and Microanalysis, 2016, 22, 186-187.	0.4	0
699	Physical Properties of Composites. , 2016, , .		0
700	Correlative Microscopy Application in Spinal Cord Injury Research. Microscopy and Microanalysis, 2016, 22, 204-205.	0.4	0
701	On compression and damage evolution in PTFE and PEEK. AIP Conference Proceedings, 2017, , .	0.4	0
702	Special Issue on â€~Modern Imaging Techniques in Fracture and Damage Analyses': Selected papers from the 21st European Conference of Fracture (ECF 21), held in Catania, Sicily, Italy, on 20–24 June 2016. Engineering Fracture Mechanics, 2017, 183, iii-iv.	4.3	0

#	Article	IF	CITATIONS
703	3D elemental mapping of materials and structures by laboratory scale spectroscopic X-ray tomography. Journal of Physics: Conference Series, 2017, 849, 012013.	0.4	0
704	4.10 Residual Stresses in Metal Matrix Composites. , 2018, , 275-286.		0
705	Post-fatigue Investigation of SLM Ti64 Scaffolds by 3D Correlative Tomography. Microscopy and Microanalysis, 2020, 26, 424-425.	0.4	Ο
706	Complementary time-lapse datasets of x-ray computed tomography and real-time strain mapping for an ex-situ study of non-crimp glass fibre composites under fatigue loading. Data in Brief, 2021, 37, 107157.	1.0	0
707	Collaborative Virtual Research Environment To Support Integration & Steering of Multi-site Experiments. , 2006, , 120-125.		Ο
708	On the Three-Dimensional Microstructure of Martensite in Carbon Steels. , 0, , 19-24.		0
709	Elastic and Thermoelastic Properties of Brittle Matrix Composites. , 2016, , .		Ο
710	Mid-thickness studies of the stress intensity factor in the bulk of bainitic steel. Frattura Ed Integrita Strutturale, 2017, 11, 203-210.	0.9	0
711	Versatile regularisation toolkit for iterative image reconstruction with proximal splitting algorithms. , 2019, , .		Ο
712	Damage Evaluation in 3D Woven Composites with Warp-way and Weft-way Binders. , 2022, , .		0